Student thesis series INES nr 761

Identifying PFAS transport pathways during pluvial flooding using surface water modelling in Gorsingeholm

Emma Wennberg

2026
Department of
Earth and Environmental Sciences
Lund University
Sölvegatan 12
S-223 62 Lund
Sweden

Emma Wennberg (2026). **Identifying PFAS transport pathways during pluvial flooding using surface water modelling in Gorsingeholm.**

Master degree thesis, 30 credits in Physical Geography and Ecosystem Science
Department of Earth and Environmental Sciences, Lund University

Level: Master of Science (MSc)

Course duration: *January* 2026 until *June* 2026

Cover picture: Raw water from Mälaren pumped into Gorsingeholm infiltration basin for MAR. Photo by Emma Wennberg, 9 April 2026.

Disclaimers

This document describes work undertaken as part of a program of study at the University of Lund. All views and opinions expressed herein remain the sole responsibility of the author, and do not necessarily represent those of the institute.

This published version of the thesis is a masked version and therefor slightly different then the examined thesis. The thesis contained confidential data and information provided by Eskilstuna Strängnäs Energi & Miljö. Some figures and detail information have thereto been removed or generalised.

Identifying PFAS transport pathways during pluvial flooding using surface water modelling in Gorsingeholm

---

Emma Wennberg

Master thesis, 30 credits, in *Physical Geography and Ecosystem Science*

Andreas Persson
Department of Earth and Environmental Science

Jonas Bermin
WSP

Thesis evaluator:
Harry Lankreijer

Course examiner:
Martin Berggren

Abstract

Per- and polyfluoroalkyl substances (PFAS) pose severe global risks to drinking water due to their persistence and high aquatic mobility. At the Gorsingeholm water treatment plant in Strängnäs, Sweden, PFAS concentrations in raw intake water from Lake Mälaren exhibited low concentrations yet spiked to heightened levels following initial artificial infiltration for managed aquifer recharge (MAR). Because the basin infiltration materials themselves were uncontaminated, this study aimed to investigate the unknown surface runoff and depression-focused groundwater recharge pathways connecting surrounding land uses (LUs) to the water treatment plant. Hydrological modelling for 10- and 100-year rain events was conducted using ArcGIS Pro, and two modelling methods; PluvioFlow and a re-creation of SCALGO Live's methodology within ArcGIS Pro. The hydrological findings were subsequently cross-referenced with industry-specific PFAS usage identified in scientific literature

Hydrological findings reveal that surface runoff watersheds contributing to the water treatment plant generally expand as the analysed buffer area increases. Runoff most likely originates from LUs to the southeast, specifically a cereal industry and a farmstead/SME property. However, under the largest analysed precautionary buffer zone, runoff pathways extended up to 8 km southwest, incorporating vast agricultural fields. Conversely, potential groundwater recharge zones generally exhibit larger spatial extent during the 100-year rain event and are heavily concentrated within flat agricultural fields. Volumetrically, two massive agricultural fields dominate the total potential groundwater infiltration largely due to their sheer spatial scale. However, smaller LU areas also contribute substantial total infiltration volumes due to high infiltration intensities relative to their size.

Integrating these identified water pathways with scientific literature on land use specific PFAS signatures highlights potential risk profiles. The cereal industry is associated with potential ground pollution and pesticide applications, while the Farmstead/SME may be associated with PFAS contamination in soil and sediments. Furthermore, agricultural fields present risks via application of sewage sludge and specific pesticide treatments.

While the measured concentrations are overall low, and a definitive point source could not be isolated, the study's aim of providing insight about potential PFAS pathways and sources, via surface runoff and groundwater recharge, were fulfilled. Ultimately, this research identifies the cereal industry (primarily via surface runoff) and the farmstead/SME (via both runoff and recharge) as the highest priority targets for future empirical sampling.

Key words: Physical geography, PFAS, Drinking water, Managed Aquifer Recharge (MAR), Pluvial flooding, Surface runoff, Groundwater recharge, PluvioFlow, SCALGO, Hydrological modelling, GIS

Sammanfattning

Per- och polyfluorerade alkylsubstanser (PFAS) utgör en allvarlig global risk för dricksvatten på grund av sin persistens och höga mobilitet i vattenmiljöer. Vid Gorsingeholms vattenverk i Strängnäs uppvisade PFAS-koncentrationerna i råvattnet från Mälaren låga koncentrationer, men uppvisade förhöjda nivåer efter artificiell infiltration för grundvattenbildning (MAR). Eftersom infiltrationsmaterialet i bassängerna bedömdes vara föroreningsfritt, syftade denna studie till att undersöka potentiell spridning via ytavrinnings- och grundvattenbildningsvägar som förbinder kringliggande markanvändning med vattenverket. Hydrologisk modellering för 10- och 100-årsregn utfördes i ArcGIS Pro och med två modellmetoder; PluvioFlow samt en återskapad metodik baserad på SCALGO Live. De hydrologiska resultaten jämfördes därefter med branschspecifik PFAS-användning identifierad i myndighetsdokument och vetenskaplig litteratur.

Resultaten visar att de avrinningsområden som bidrar till vattenverket generellt expanderar i takt med att den analyserade buffertzonen ökar. Ytavrinning härrör sannolikt främst från markanvändning i sydost, specifikt en spannmålsindustri och en jordbruksfastighet/SMF. Vid den största analyserade buffertzonen sträckte sig avrinningsvägarna upp till 8 km åt sydväst och inkluderade omfattande jordbruksmarker. Potentiella grundvattenbildningsområden uppvisar generellt en större rumslig utbredning vid 100-årsregn och är starkt koncentrerade till flacka åkermarker. Volymmässigt domineras den totala potentiella grundvattenbildningen av två stora åkermarker, främst på grund av deras betydande yta. Mindre markanvändningsområden bidrar dock också med substantiella infiltrationsvolymer tack vare hög infiltrationsintensitet i förhållande till deras storlek.

Genom att integrera dessa identifierade vattenvägar med vetenskaplig litteratur gällande branschspecifik PFAS-användning för olika markanvändningstyper och aktiviteter framträder potentiella riskprofiler. Spannmålsindustrin förknippas med potentiell markförorening och pesticid-användning, medan jordbruksfastigheten/SMF-verksamheten kan vara kopplad till PFAS-föroreningar i jord och sediment. Vidare utgör åkermark en risk genom potentiell spridning av avloppsslam och specifika bekämpningsmedel.

Även om de uppmätta koncentrationerna är låga och en specifik punktkälla inte kunde isoleras, har studiens syfte att ge ökad insikt om potentiella PFAS-vägar och källor via ytavrinning och grundvattenbildning uppfyllts. Sammanfattningsvis identifierar denna forskning spannmålsindustrin (främst via ytavrinning) och jordbruksfastigheten/SMF-verksamheten (via både avrinning och grundvattenbildning) som högprioriterade områden för framtida empirisk provtagning.

Nyckelord: Naturgeografi, PFAS, Dricksvatten, Managed Aquifer Recharge (MAR), Skyfallsöversvämning, Ytavrinning, Grundvattenbildning, PluvioFlow, SCALGO, Hydrologisk modellering, GIS

Table of Contents

List of Abbreviations

BKL	Bransch Klass
CDS	Chicago Design Storm
DEM	Digital Elevation Modell
IDF	Intensity-Duration-Frequency
LM	Lantmäteriet
LU	Land Use
MAR	Managed Aquifer Recharge
MFD	Multiple flow direction
NVV	Naturvårdsverket
PFAS	Per- and polyfluoroalkyl substances
RH2000	Rikets höjdsystem 2000
SFD	Single flow direction
SGU	Sveriges Geologiska Undersökning
SME	Small-Medium Enterprise
SMHI	Sveriges Meteorologiska & Hydrologiska Institut
TFM	Triangular form-based multiple flow
TV	Trafikverket
WSP	Williams Sale Partnership

Full list of all PFAS compounds mentioned in this text can be found in Appendix

Acknowledgements

First and foremost, I would like to thank my supervisors, Andreas Persson and Jonas Bermin, for their invaluable guidance, support, and ideas throughout this process. I am also grateful to Sofia Nyholm for connecting me with Jonas and helping get a foot into this project. A special thank you to the team at PluvioFlow for their assistance with the modelling software, and to Jonas Lindberg at ESEM for the insightful tour of the Gorsingeholm water treatment plant. Finally, I would like to extend my thanks to WSP and ESEM for allowing me to partake in this project.

1 Introduction

Per- and polyfluoroalkyl substances (PFAS), often referred to as “forever chemicals”, represent a widespread global environmental and public health challenge (Ackerman Grunfeld et al., 2024; Brusseau et al., 2020). PFAS compounds have been found in low but measurable concentrations all over the globe, even in remote locations far from any potential source (Brusseau et al., 2020). Their high resistance to thermal, chemical, and biological degradation ensures their persistence in both industrial applications and natural ecosystems (Earon, 2025; European Chemical Agency, n.d.; KEMI, 2026b). Because of their unique chemical properties, PFAS are highly mobile in aquatic environments, enabling them to be transported across vast distances via groundwater and surface water (Earon, 2025). A study made by Rico et.al. (2026) during the 2024 flash flood in Valencia, Spain, concluded that PFAS concentrations surged in downstream aquatic ecosystems post-flood (Rico et al., 2026). This was partly because the water transportation was particularly amplified during pluvial flooding events, where rapid runoff could remobilise PFAS pollutions and facilitate their entry into critical water supplies (Rico et al., 2026). Given their bioaccumulative potential, the lack of efficient remediation methods, documented toxic effects, including endocrine disruption and suspected carcinogenicity, the presence of PFAS in drinking water constitutes a primary risk to human health (Ackerman Grunfeld et al., 2024; Earon, 2025; European Chemical Agency, n.d.; KEMI, 2026b). Therefore, regulatory bodies have established stringent limits to safeguard public and ecosystem health (Livsmedelsverket, 2026). In Sweden, the PFAS4 and PFAS21 groups are subject to legally binding drinking water limits of 4 and 100 ng/L, respectively (LIVSFS 2022:12, 2023).

The Gorsingeholm water treatment plant in Strängnäs Municipality serves as a critical example of the complexities inherent in PFAS source tracking. The facility functions as a backup for municipal drinking water, utilising a two-step artificial infiltration process where raw surface water from Lake Mälaren is pumped into infiltration basins for managed aquifer recharge (MAR) to supplement the naturally occurring groundwater in the fluvioglacial Strängnäsåsen aquifer (Maldonado & Tagesson, 2025). The first infiltration step takes place on the water treatment plant premises in the northern area, while the second infiltration step is located a few hundred meters south in the southern area (Maldonado & Tagesson, 2025).

Current monitoring reveals that while the raw intake water contains low PFAS levels, PFAS4 concentrations spike to heightened levels following the first infiltration step, only to decrease slightly after the second infiltration step (Bermin, 2025). This discrepancy raises the question of where the PFAS contamination originates. At the same time, the slight decrease after the second infiltration step (located further south) suggests that PFAS is being mobilised from the surrounding landscape or subsurface in direct proximity to the water treatment plant in the north. Therefore, the main focus in this report is on the water processes in between the two PFAS measuring points with heightened concentrations, and what may affect the first infiltration step in the north more than the second infiltration step in the south.

The consulting company WSP has conducted PFAS measurements in the study area. However, due to the complexity of the hydrological system, the source(s) of contamination have not yet been clearly identified. Analyses of infiltration basin media indicate that the elevated PFAS concentrations do not originate from the infiltration material itself (Bermin, 2025). This suggests that PFAS may be entering the infiltration system via groundwater or surface water flow from surrounding areas. While groundwater level and flow direction are monitored, the surface water flow and groundwater recharge patterns in the immediate surroundings remain largely unknown, making it difficult to identify which land use(s) or activities are contributing to the chemical load.

This study seeks to fill this gap by testing the idea that the PFAS contamination at Gorsingeholm is "activated" by specific hydrological pathways that only become prominent during extreme rainfall. To achieve this, the research employs an evaluative modelling approach, comparing the two models, SCALGO (static) and PluvioFlow (dynamic). By simulating 10-year and 100-year rain events, the study identifies where rainfall is most likely to infiltrate into the groundwater or migrate as runoff. The decision to model hydrological pathways during extreme rainfall was partly based on Rico et al.´s findings after the Valencia flood (2026), and partly due to the limited and inconsistent PFAS measurements available, making them less useful for a direct analysis of whether the potential source is a one-time occurrence or a long-term cumulative inflow.

The expectation is that by comparing a static model (which assumes instantaneous capacity) with a dynamic model (which accounts for timing and saturation), the study will reveal how land use activities do or do not become hydrologically connected to the study area during storm events. Allowing for a "source-to-sink" analysis that links physical water movement to land use and industry-specific PFAS usage.

1.1 Aim and Research Questions

The overall aim of this study is to improve the understanding of surface water flow patterns and groundwater recharge zones in the area and to connect those findings with potential neighbouring PFAS-associated land uses and activities, providing valuable insight about potential PFAS pathways and sources. The study will address the aim by answering the following research questions:

1. *What surface runoff and potential groundwater recharge patterns exist within the study area and its proximity?*
    a. *From where could surface runoff to the study area originate?*
    b. *What is the spatial distribution of groundwater recharge zones during rainfall events with medium to long return periods?*
2. *Which land uses are located within the surface runoff paths and recharge zones, potentially contributing water to the infiltration basins for MAR in the study area during different rainfall events?*
    a. *How large are the areas of the surface runoff and recharge zones within each identified land use?*
    b. *What volumes of water are infiltrated into the soil or groundwater within each land use area?*
3. *What PFAS usage are the identified land uses associated with, according to the scientific literature?*

1.1.1 Delimitations

To maintain a focused investigation into the potential PFAS transport pathways at Gorsingeholm, a few delimitations had to be established. Firstly, the study is delimited to the comparison of two models, SCALGO and PluvioFlow. This choice was made to contrast a widely used static screening tool with a newly developed dynamic model, rather than conducting an exhaustive review of all available hydrological software. The decision to use two models was primarily to evaluate the trustworthiness of the results. Secondly, the study is delimited to the simulation of two different extreme rain events, namely 10- and 100-year return periods, respectively. These were chosen since they represent quite extreme events with high hydrological stress able of capturing the waterflow in the study area, and capable of activating transport pathways that may remain dormant during average precipitation. Climate factors or the effects of seasonal snowmelt are not included.

An important reservation must be made regarding the groundwater recharge zones identified in this study, which represent areas of potential recharge rather than confirmed hydrogeological pathways. Since subsurface analysis was excluded from the scope, no definitive conclusions can be drawn concerning whether these surface depressions are hydrologically connected to the specific aquifer feeding the MAR infiltration basins. Furthermore, without geological verification of whether the local aquifers are confined or unconfined, surface infiltration cannot be assumed to translate directly into aquifer storage.

It should be noted that while this study maps hydrological connectivity to various land uses, the assessment of PFAS association is based on broad industry categories found in literature. This report does not conduct on-site contamination verification for the identified land uses and activities. Consequently, the discussion regarding whether a specific land use is associated with PFAS must be interpreted as an assessment of risk potential and a guide for further investigation, rather than a confirmed diagnosis of the local contamination source.

2 Background

The conceptual framework for this study follows a Source-Path-Receptor model. While the receptor (drinking water from the study area) is identified, the specific sources and paths remain unknown. This section establishes the theoretical basis for PFAS behaviour, and the hydrological modelling used to identify these missing links.

2.1 PFAS

Per- and polyfluoroalkyl substances (PFAS) comprise a large and highly diverse group of synthetic chemicals, with more than 10,000 identified substances (European Chemical Agency, n.d.). All PFAS are anthropogenic and do not occur naturally in the environment. Due to their physicochemical properties, they have been widely used in industrial and consumer products for decades, most notably in e.g. aerospace and defence, firefighting foams, electronics, textiles, and food contact materials (Earon, 2025; European Chemical Agency, n.d.; Glüge et al., 2020).

The environmental and human health impacts of PFAS are increasingly recognised as serious, particularly due to their persistence, mobility, and bioaccumulative potential (Earon, 2025). Certain PFAS are known to accumulate in humans, animals, and plants and may cause toxic effects, including reproductive toxicity, developmental effects, endocrine disruption, and suspected carcinogenicity (European Chemical Agency, n.d.; KEMI, 2026b). Although only a limited number of PFAS have been thoroughly studied, there are strong reasons to consider the entire group as potentially hazardous (KEMI, 2026b).

2.1.1 Chemical Structure & Persistence

All PFAS contain the common structure of a fully (per-) or partially (poly-) fluorinated carbon chain, which is hydrophobic, and some functional group, which typically is hydrophilic (European Chemical Agency, n.d.; KEMI, 2026b; Sparrenbom & Jeppsson, 2022). The carbon-fluorine bond, present in PFAS, is one of the strongest chemical bonds in organic chemistry, which explains their exceptional chemical and thermal stability (European Chemical Agency, n.d.). PFAS are stable under intense heat and resistant to hydrolysis, photolysis, and biodegradation (European Chemical Agency, n.d.; KEMI, 2026b), and are commonly referred to as "forever chemicals" because of this extreme persistence. Some PFAS do not degrade at all, while others transform into other PFAS compounds; however, complete degradation under environmental conditions has not been observed (KEMI, 2026b). If releases continue, PFAS will continue to accumulate in environmental compartments, including drinking water and food chains (European Chemical Agency, n.d.).

2.1.2 Chain length – Solubility & Sorption

The transport behaviour of PFAS is largely dictated by their carbon chain length and functional groups (Li et al., 2023). In general, the chemical properties of these substances shift as the chain length increases, becoming increasingly hydro- and lipophobic. This occurs because the hydrophilic functional group has a diminished effect relative to the hydrophobic fluorinated chain as the molecule grows, thereby decreasing its water solubility (Li et al., 2023).

According to Buck et.al.'s classification of PFAS compounds from 2011, long-chained PFAS are categorised as perfluoroalkyl carboxylic acids (PFCAs) with eight or more carbon atoms, perfluoroalkane sulfonic acids (PFSAs) with six or more carbon atoms, and other PFAS variants with seven or more carbons (Buck et al., 2011). Long-chain compounds, such as PFNA, PFOS, and PFHxS, exhibit lower water solubility and tend to sorb to solid materials to a higher degree than their short-chain counterparts (Dalahmeh et al., 2018; Sparrenbom & Jeppsson, 2022). Conversely, short-chain PFAS exhibit higher water solubility and lower partitioning to the solid or organic phases, making them significantly more mobile in soil and groundwater (Kannan et al., 2026; Sparrenbom & Jeppsson, 2022).

Because many PFAS compounds remain largely dissolved, it would imply that PFAS exhibit high mobility during storm events and therefore be transported over long distances through both surface and groundwater systems.

2.1.3 PFAS Regulations – Guidelines- and Limit Values

To manage the complexity of the thousands of individual substances, regulatory bodies group PFAS into sum parameters based on chemical similarities. This study focuses primarily on the PFAS4 and PFAS21 groups, as these form the basis for current Swedish drinking water regulations (LIVSFS 2022:12, 2023).

The determination of "acceptable" PFAS concentrations is a complex process, resulting in a variety of limits and guidelines issued by different Swedish agencies for different media, such as soil, groundwater, surface water, and drinking water (KEMI, 2024a). It is important to distinguish between limit values, which are legally binding, and guidelines, which are only directive or indicative for environmental quality. The primary focus of this study is the two legally binding drinking water limits, established through the regulation "*Livsmedelsverkets föreskrifter om dricksvatten – LIVSFS 2022:12*" by the Swedish National Food Agency (*Livsmedelsverket*), presented in Table 1 (LIVSFS 2022:12, 2023). Livsmedelsverket's regulations of PFAS21 are national implementations of the EU drinking water directive (Directive 2020/2184, 2020) regulating PFAS20, with the addition of 6:2 FTS, making it a sum of 21 PFAS compounds. The 4 ng/L limit for PFAS4 which is based on EFSAs (European Food Safety Authority) assessment from 2020 concerning tolerable intake of PFAS4 (EFSA CONTAM Panel et al., 2020), an assessment the drinking water directive did not account for.

Table 1. Assessment criteria for PFAS in drinking water (Adapted from LIVSFS 2022:12, 2023). Full names of all compounds can be found in Appendix.

Type of sample	Group	Included compounds	Concentration	Comment
Drinking water	PFAS4	PFOA, PFNA, PFOS and PFHxS	4 ng/L	Legally binding from 1/1-2026.
	PFAS21	Above-mentioned PFAS4 compounds and PFBA, PFPA, PFHxA, PFHpA, PFDA, PFUnDA, PFDoDA, PFTrDA, PFBS, PFPS, PFHpS, PFNS, PFDS, PFUnDS, PFDoDS, PFTrDS and 6:2 FTS	100 ng/L	

As a point of comparison, it should be noted that PFAS are already widely distributed throughout the Swedish environment. This dispersal occurs continuously and diffusely through precipitation, as well as through localised point sources such as emissions or leakage. Consequently, background concentration levels in drinking water source areas have been measured at an average of 8.4 ng/L for a sum of 26 different PFAS compounds (Ahrens et al., 2016). A study made by Cousins et.al. presents findings of approximately 1-2 ng/L of PFAS4 in rain water in rural and urban regions in Sweden (Cousins et al., 2022). In groundwater the average PFAS concentrations ranges from 1-100 ng/L and is approximately double the concentration found in surface water (Shah et al., 2025).

2.1.4 PFAS in Hydrology, Hydrogeology and Geology

The transport of PFAS through the environment is strongly linked to the movement of water. Because of their hydrophilic part, they are readily transported in the dissolved phase, allowing them to follow the natural pathways of the water cycle from surface runoff down into groundwater aquifers (ITRC, 2023).

Recent studies identify leaching from contaminated topsoil and transportation by surface flow due to precipitation as a possible PFAS contamination pathway (Borthakur et al., 2021; Dauchy et al., 2019; Richardson et al., 2022). Because many types of PFAS, particularly short-chain compounds, exhibit low affinity for suspended sediments, they remain in the aqueous phase rather than settling out (Sparrenbom & Jeppsson, 2022). This enables rapid, long-distance downstream transport during high-intensity rainfall, making surface runoff a critical pathway for the spread of contamination from point sources to wider areas.

When water infiltrates the ground, it may carry dissolved PFAS through the unsaturated soils. The geological composition of the aquifer influences the transportation of PFAS (Ahmed et al., 2020; Li et al., 2023). Conversely, in areas with significant clay content or organic matter, certain compounds may be partially immobilised through sorption of the hydrophobic part, while others continue to move at nearly the same velocity as the groundwater itself (ITRC, 2023). Furthermore, PFAS are known to accumulate at the air-water interface, e.g. within the pore spaces of unsaturated soils (ITRC, 2026), and it has been shown that PFAS are retained at high concentrations in this unsaturated zone, ranging up to several hundred mg/kg for PFOS in contaminated sites (Brusseau et al., 2020). This behaviour can retard their movement compared to the speed of the infiltrating water, effectively creating a long-term reservoir of contamination in the unsaturated zone.

Once PFAS reach the groundwater table, their transport is governed by hydrogeological processes such as advection, dispersion and diffusion (ITRC, 2023). Advection, i.e. the movement of a compound within water without reducing concentrations along the flow path, is often the driver of PFAS mobility (ITRC, 2023). Minor velocity changes in surface water can disperse contaminants in multiple directions, driving vertical mixing and cross-media transport, e.g. from surface water to sediment (ITRC, 2023). Diffusion, which is the movement of molecules in response to a concentration gradient, is often slow in groundwater compared to advection (ITRC, 2023). The diffusion of contaminant mass into lower-permeability materials like clays or bedrock may sequester PFAS within the subsurface, serving as a long-term source of PFAS to the groundwater (ITRC, 2023).

2.3 Hydrological Modelling

Hydrological modelling is used to simulate the movement of water across a landscape, which in the context of this study serves as the primary transport mechanism for PFAS. To accurately represent these processes, the model must account for the characteristics of the precipitation event, the physical rules governing water flow, and the temporal nature of the flood.

2.3.1 Cloudbursts and Chicago Design Storms (CDS)

A cloudburst is an extreme precipitation event defined by high intensity over a short duration (SMHI, n.d.-a). One way to categorise the level of extreme events, such as cloudbursts, in a defined location is with return periods, e.g., 10-year or 100-year events (AMS, n.d.). Return periods are a measure of the statistical probability of an occurrence of equal or greater magnitude, based on historical data (AMS, n.d.; Rakhecha & Singh, 2010), and are often used for risk analysis (Koliokosta, 2023). Consequently, a longer return period, such as 100 years, indicates a rain event with a magnitude extreme enough to only occur once in a hundred years, while a 10-year event is of a lower magnitude and thus statistically likely to occur more often.

One way to simulate cloudbursts is to design synthetic rain events, and a widely used method in urban environments is the Chicago Design Storm (CDS), first proposed by Keifer and Chu in 1957 (Keifer & Chu, 1957; Lopes da Silveira, 2016; SCALGO, 2024). It constructs a synthetic storm hyetograph based on local Intensity-Duration-Frequency (IDF) data (Lopes da Silveira, 2016; SCALGO, n.d.-a). Unlike a uniform block of rain, a CDS rain places the peak intensity at a specific point (usually at the middle of the event) to realistically simulate how a catchment responds to a sudden surge of water (SCALGO, n.d.-a).

2.3.2 Flow Algorithms (SFD, MFD & TFM)

Earlier flow-routing models were relatively simple in that water was passed from a cell to one or several neighbouring cells solely on the basis of elevation differences (Tarboton, 1997), following either a single-flow-direction (SFD) like the D8-model or a multiple-flow-direction (MFD) approach (Persson et al., 2024). Lea (1992) advanced this idea by allowing each pixel to be assigned its own slope and aspect, which determine the direction(s) in which water should flow from that pixel. Building on these developments, Tarboton (1997) introduced a new method for calculating flow direction based on subdividing each cell into eight triangular facets with individual aspects.

Based on MFD algorithms, Pilesjö & Hasan (2014) proposed the triangular form-based multiple flow (TFM) algorithm. In this algorithm, flow redistribution is modelled by subdividing the central cell within a 3x3 cell neighbourhood into eight triangular facets radiating from the cell centre (Persson et al., 2024). Each grid cell in the DEM is treated in turn as the focal cell to estimate the flow from that cell. The eight facets align with the eight surrounding cells in the 3x3 neighbourhood, and each facet represents a directional unit through which water can accumulate and potentially flow. For every facet, the algorithm evaluates the local aspect (downslope direction) to determine whether the stored water remains within the facet, moves entirely toward one adjacent cell, or splits between the two neighbouring cells that share that facet boundary. After this facet-level assessment, the accumulated water is routed to the appropriate neighbouring cells based on their relative elevations. If both cells adjacent to a facet are higher than the central cell, but other cells in the surrounding neighbourhood are lower, the algorithm reallocates the facet's water proportionally toward those lower-elevation cells to preserve physically realistic downslope flow (Persson et al., 2024). The TFM algorithm can be applied in both static and dynamic flow models, and one dynamic application is the TFM-DYN algorithm, where all calculations are performed in each timestep as a reaction to previous stages continuously (Persson et al., 2024).

2.3.3 Static vs. Dynamic Flood Modelling

Hydrological models are generally categorised based on how they treat the variable of time and the physical movement of water. Static models are primarily concerned with the final distribution of water based on topography, whereas dynamic models simulate the physical progression of a flood wave across the landscape through time (Persson et al., 2024). While static models are computationally efficient for large-scale screening, dynamic models provide the temporal resolution necessary to understand flow velocities and the momentum of moving water (Guo et al., 2021; Persson et al., 2024).

2.3.3.1 SCALGO Live Flash Flood Map

SCALGO utilises a "fill-and-spill" approach with an SFD-algorithm, which is a stationary model simplifying the natural process for screening purposes (SCALGO, n.d.-c). This method is highly effective for identifying topographical depressions where water will pool, though it does not consider the duration of the rain event, since it assumes the specified rainfall is immediately available on each cell (SCALGO, n.d.-c). The simulation routes the specified water volume downstream, filling depressions on the way, and if a depression's volume is exceeded, the remaining water continues to the next depression downstream (SCALGO, n.d.-c).

The SCALGO Live Flash Flood Map has the option to utilise runoff functions, subtracting part of the rainfall as infiltration before the rest continues downstream as runoff (SCALGO, n.d.-c). Surface runoff is then quantified at a pixel-based level by integrating high-resolution land cover data with localised design storm profiles (SCALGO, 2024). Water surfaces are assigned a 100% runoff coefficient (SCALGO, 2024). Natural surfaces have runoff calculated as rainfall minus infiltration, with rates assessed based on soil type and land cover condition (SCALGO, 2024). Artificial surfaces have losses determined by the capacity of underground drainage systems, i.e. where a system is present, runoff equals rainfall minus capacity, while surfaces without a system result in 100 % runoff (SCALGO, 2024). For these runoff functions, the model employs a modified pixel-based version of the traditional Soil Conservation Service (SCS) Curve Number (CN) method, designated as CN-p (SCALGO, 2024). Furthermore, SCALGO's version of CN addresses specifically true surface runoff, and not subsurface flows (SCALGO, 2024). For precipitation data, SCALGO typically uses the Chicago Design Storm (CDS) method, utilising national IDF-tables based on Dahlström (2010) and the Svenskt Vatten report P110 from 2016 (Dahlström, 2010; SCALGO, 2024; Svenskt Vatten, 2016).

2.3.3.2 PluvioFlow

PluvioFlow is a dynamic hydrological modelling tool designed for detailed cloudburst mapping utilising the TFM-DYN algorithm (see section 2.3.2) to distribute water over terrain and time, accounting for the momentum of water and how infiltration rates change as the soil becomes saturated (Persson et al., 2024; PluvioFlow, 2026b). The modelling process integrates infrastructure data from Swedish authorities and open sources with the input digital elevation model (DEM) to generate a hydrologically corrected elevation model where buildings are raised by 3 meters and critical infrastructure, such as bridges and culverts, are integrated into the terrain to ensure realistic flow paths (PluvioFlow, 2026b). PluvioFlow creates CDS events based on total rain with different return periods and durations from SMHIs cloudburst statistics (Olsson et al., 2017; SMHI, n.d.-b, 2017). The cloudburst statistics are based on SMHIs approximately 130 automatic weather stations, reporting rainfall every 15th minute, around the country (Olsson et al., 2017; SMHI, n.d.-b, 2017).

During simulation, PluvioFlow applies dynamic infiltration modules to over 30 different land cover types (PluvioFlow, 2026b). It employs a two-stage approach where a cell maintains a specific "pre-infiltration" capacity until it reaches a 90 % saturation threshold, at which point it shifts to a lower "post-infiltration" rate (PluvioFlow, 2026b). Surface friction is managed via Manning's roughness coefficients, while movement through urban infrastructure is calculated using hydraulic formulas for pipe and pressure flow to account for culverts and drainage systems (PluvioFlow, 2026b). Because the model is dynamic, it produces comprehensive, time-dependent outputs, including water depth, momentum, animated particle flow paths, and the total duration of flooding (PluvioFlow, 2026b).

3 Method

The project combined hydrological modelling, spatial analysis, and literature review to address the research questions.

A watershed analysis was performed in ArcGIS Pro version 3.2.0 to identify surface flow patterns (Esri, 2023a), while flash flood modelling was performed to identify groundwater recharge zones during 10- and 100-year rain events. To evaluate the validity of the results, the flash flood modelling was performed using two models (PluvioFlow version 2026.03.19 & SCALGO Live). To get a harmonized output, the use of SCALGO's software was partly combined with a re-creation of its methodology in ArcGIS Pro. Model outputs were used to identify zones contributing to surface runoff and groundwater recharge for each rainfall event. These zones were then overlaid with land-use data to identify industries and activities potentially contributing with PFAS-contaminated water during different rain events. Area of runoff and recharge zones, as well as the infiltrated volumes of water from recharge zones, will be calculated per land use. Finally, a literature review was conducted to identify PFAS compounds commonly associated with each land use type.

3.1 Data

The data sources used by PluvioFlow (version 2026.03.19) to prepare simulation scenario layers for both 10-year and 100-year rain events can be found in Table 2. The generated CDS-rains making out the extreme precipitation data are based on SMHIs cloudburst statistics for southeast Sweden (Olsson et al., 2017; SMHI, 2025). Date refers to when the dataset was brought into the PluvioFlow platform.

Table 2. Data sources used for flood modelling in PluvioFlow. Table provided by the PluvioFlow Simulation Reports (PluvioFlow, 2026a), with the addition of the precipitation data (PluvioFlow, 2026b).

Layer	Source	Organisation	Date	Description
Precipitation	Based on SMHI weather stations	SMHI	*	Generated CDS-rain, based on SMHI:s extreme rain statistics
Blues i.e. waterbodies including lakes, seas, rivers, streams, and coastal areas.	Vattenatlas Kustvattenområden 2022	LM	*	Coastal water areas (Sweden), 2022 edition.
	OpenStreetMap (Sweden)	OpenStreet-Map	*	OSM database extract covering Sweden.
	SMHI Hydrografi	LM	*	SMHI Hydrografi
Greens i.e. vegetated and pervious surfaces including parks, forests, lawns, gardens, agricultural land, and green infrastructure.	Nationella Marktäckedata (NMD)	NVV	*	Swedish national land cover dataset (Naturvårdsverket).
	OpenStreetMap (Sweden)	OpenStreet-Map	*	OSM database extract covering Sweden.

Greys i.e. impervious surfaces such as roads, streets, parking lots, sidewalks, plazas, and other paved areas.	Trafikverket NVDB	TV	Nov 13, 2025	National Road Database (NVDB) for Sweden.
Buildings	Lantmäteriet Buildings	LM	*	Building footprints as vector data via STAC.
Surface i.e. DEM	Nationell Höjdmodell (NH)	LM	*	Sweden national elevation model from Lantmäteriet.
Soils	SGU Jordarter	SGU	Nov 13, 2025	Quaternary deposits / soil types from SGU.
Culverts	Trafikverket Trummor	TV	Nov 13, 2025	Culverts (vägtrummor), likely from NVDB.
Bridges	pf_generate_bridges	-	*	-

*Latest accessible data (as of 2026-04-07)

The data sources used by SCALGO Live to produce the terrain model with buildings, on which the Flash Flood Map is based, can be found in Table 3. Additionally, sources for the layers *Topsoil type*, *Land Cover* and *Tätorter,* which determine the runoff functions for the Flash Flood Map, are also found in Table 3.

Table 3. Presents the data used by SCALGO Live to produce the Flash Flood Map and Runoff functions.

Layer	Organisation	Data set	Date acquired
Flash Flood Map	Scalgo	Hydrological Corrections	2026-03-06
	Lantmäteriet	Markhöjdmodell, grid 1+	2026-01-14
	Lantmäteriverket (FI)	Höjdmodell 2 m	2025-08-11
	Lantmäteriverket (FI)	Höjdmodell 10 m	2017-10-04
	Kartverket (NO)	NDH DTM1	2025-12-02
	Kartverket (NO)	DTM 10	2013-07-30
	Lantmäteriet	Hydrografi, Shoreline	2026-01-23
	Lantmäteriet	Byggnad Nedladdning	2026-01-22
Topsoil type	SGU	GE.Jordarter	2025-08-18
Land Cover	Lantmäteriet	Ortofoto Visning Årsvisa	2026-01-22
	Lantmäteriet	Hydrografi	2026-01-23
	Lantmäteriet	Byggnad Nedladdning	2026-01-22
	Trafikverket	Vägdata	2026-01-14
	OpenStreetMap	Railroads	2026-01-14
	Jordbruksverket	Jordbruksblock	2025-08-18
Tätorter	Scalgo	Land Cover	2026-03-05
	Statistikmyndigheten	Tätorter 2020	2025-10-07

3.2 Study Area

The immediate study area in this report was the water treatment plant located in Gorsingeholm, Strängnäs municipality, Sweden, indicated by a white square in Figure 1. The focus in this report is the water treatment plant facility and the infiltration basins for MAR in the northern area, since that was where the heightened PFAS concentrations were measured (see section 3.2.4). The modelled area used for flash flood simulations in PluvioFlow and SCALGO encompassed the surrounding four sub-catchments (see Figure 2 in section 3.2.1), to account for rain volumes from the whole watershed. However, the actual analysis of the simulation outputs was merely extended to a study area of approximately one kilometre around the water treatment plant.

The water treatment plant has two functions, one ordinary and one backup function. The ordinary function is to produce cooling water and to act as a pressure regulator station, distributing incoming drinking water from Stockholm to the Strängnäs community via a water tower. The backup function is to produce drinking water locally if, for any reason, the supply from Stockholm is insufficient. During this process, raw water from Mälaren is pumped in to the water treatment plant, where it undergoes the first infiltration step in any of the three primary basins located at the operative establishment. Following this, the water is pumped to the southern part of the study area to enter one of the two additional infiltration basins for MAR and a natural ridge formation for the second infiltration. Once this second step is completed, the water is pumped back to the water treatment plant to be mixed with any drinking water from Stockholm and further distributed to the network. This local production is thus derived from both infiltrated and induced surface water from Mälaren as well as natural groundwater (Maldonado & Tagesson, 2025).

Figure 1. General overview of the study system. The figure is intentionally simplified and does not display detailed locations of raw water intake, groundwater abstraction- and observation wells. The water treatment plant, i.e. the immediate study area, is marked with a white square. The second infiltration step is located just south of the ridge formation, which in turn is located south of the water treatment plant. Basemap: World Imagery [1]

3.2.1 Topography and Landscape Characteristics

The Gorsingeholm study area is situated within a distinct valley landscape characterised by a central low-lying corridor flanked by higher elevated terrain to the east and west. According to the elevation data presented in Figure 2, the central valley floor, where the water treatment plant and its infiltration basins are located, is relatively flat with elevations ranging from approximately 4 to 10 m.a.s.l. In contrast, the surrounding ridges and forested areas rise significantly, reaching elevations between 50 and 70 m.a.s.l., with the highest peaks in the broader catchment area extending up to around 100 m.a.s.l (Maldonado & Tagesson, 2025). To manage water levels in these low-lying areas, the agricultural land south of the treatment plant (*Norra området* in Figure 2) was equipped with multiple drainage ditches (Maldonado & Tagesson, 2025). Additionally, the landscape includes features such as a man-made dam located approximately 200 metres east of the southern infiltration basins (*Södra området* in Figure 2) (Maldonado & Tagesson, 2025).

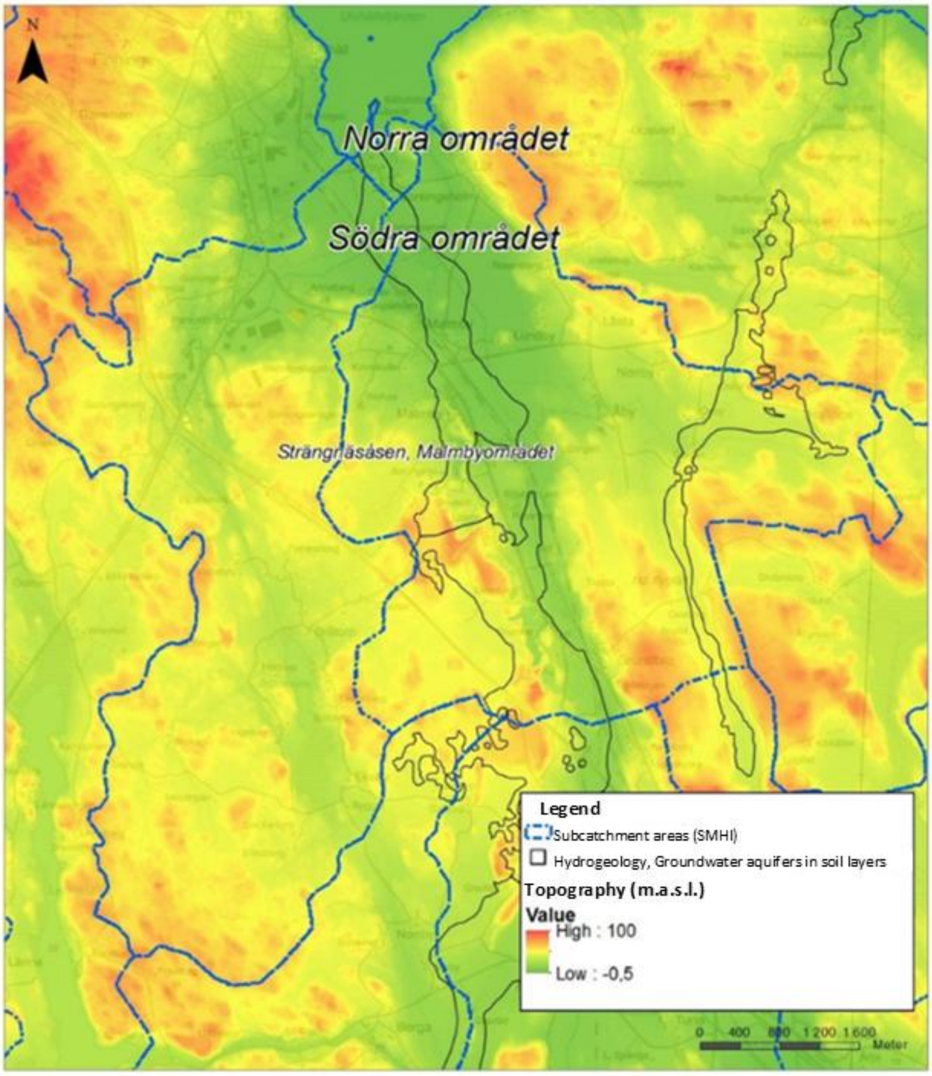

Figure 2. Elevation data over the study area. Translated to English from (Maldonado & Tagesson, 2025)*. The provider of this map has given their permission to use this figure.*

3.2.2 Geology

The geological composition of the Gorsingeholm area is defined by its position below the highest shoreline (*Högsta kustlinjen*), indicating that the entire catchment was submerged during the post-glacial period (Maldonado & Tagesson, 2025). This history has resulted in a landscape dominated by fine-grained sedimentary deposits in low-lying areas and wave-washed materials on higher ground (see Figure 3).

The deposits within the central valley primarily consist of glacial and post-glacial fine clay, as well as large accumulations of gyttja clay. A prominent glaciofluvial formation, part of the Strängnäsåsen esker, runs through the centre of the study area in a north-south direction. This esker is characterised by glaciofluvial sediments, including gravel and sand, which form a highly permeable ridge (Maldonado & Tagesson, 2025). Both the water treatment plant in the northern area (*Norra området*) and the additional infiltration basins in the southern area (*Södra området*) is strategically situated atop the esker core. Between the water treatment plant and the southern area, the glaciofluvial material is covered by a less permeable layer of soil, which influences the local hydrogeological connectivity (Maldonado & Tagesson, 2025). The terrain flanking the valley to the east and west is dominated by till and outcrops of exposed bedrock, but along the eastern slopes of the valley, there are also spots of postglacial sand and gravel, typical of areas that were subject to waves during the land uplift process (Maldonado & Tagesson, 2025).

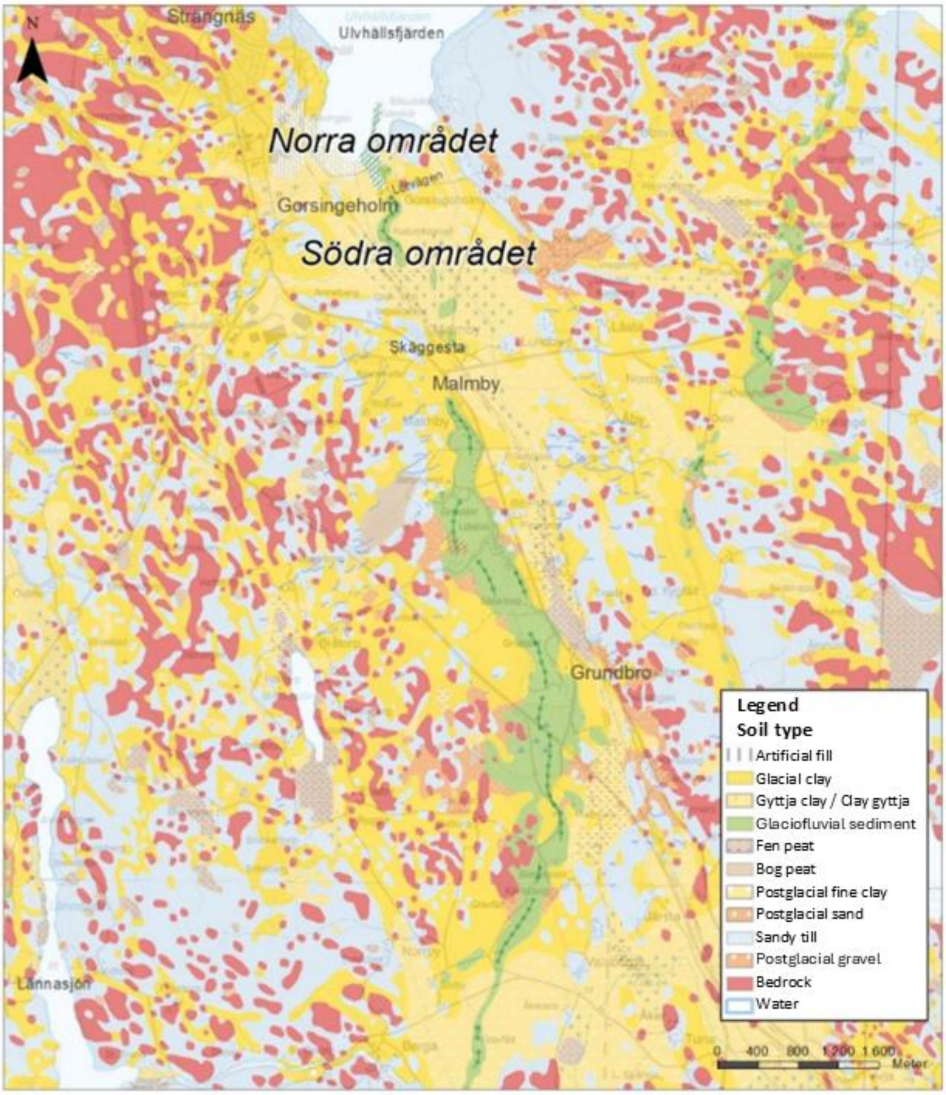

Figure 3. Geological map of the study area. Translated to English from (Maldonado & Tagesson, 2025). *The provider of this map has given their permission to use this figure.*

3.2.3 Hydrogeology

The hydrogeological conditions of the Gorsingeholm area are characterised by a dynamic groundwater system primarily hosted within the permeable glaciofluvial sediments of the esker Strängnäsåsen. The difference in groundwater levels, determining the subsurface flow direction, is primarily determined by the operational conditions, though it is also influenced by precipitation and the water levels of Lake Mälaren (Maldonado, 2021).

Geologically, the groundwater table resides within the glaciofluvial sediment layer, which is situated above the bedrock and partially confined by overlying clay in the central portion of the study area. The esker serves as a high-capacity groundwater reservoir, while the northern infiltration basins facilitate induced surface water infiltration from Mälaren (Maldonado, 2021).

3.2.4 Previous PFAS Measurements

Previous water quality assessments in the study area have identified the presence of PFAS at varying concentrations throughout the infiltration process (Bermin, 2025). As illustrated in Figure 4, raw water sourced from Lake Mälaren initially contained low levels of PFAS. However, an increase in concentrations was observed after the first infiltration step in the northern area (*Norra området*) (Bermin, 2025). Following the second infiltration step in the southern area (*Södra området*), the concentrations were still heightened but showed a slight reduction (Bermin, 2025). Despite this minor decrease toward the end of the treatment chain, the concentrations remained elevated compared to the original raw water source. This trend suggests a potential mobilisation of PFAS pollution from the ground or subsurface within or in direct proximity to the northern area.

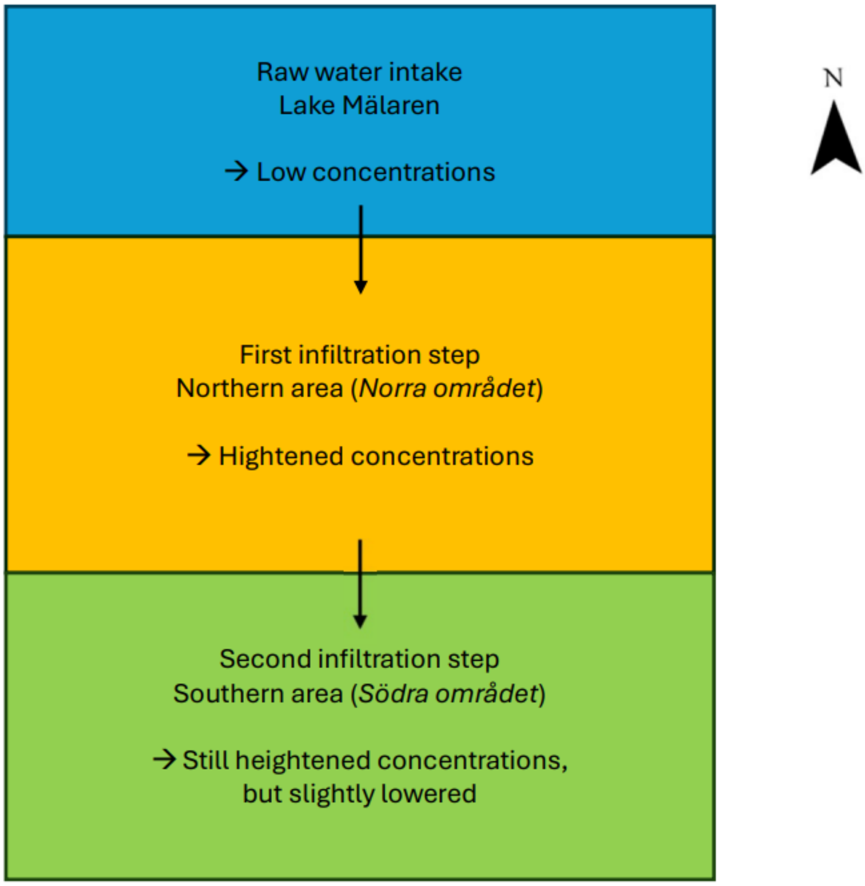

Figure 4. Principle sketch showing overall PFAS concentration trends through the system: low in raw water, elevated after the first infiltration step, and somewhat lower after the second step. The figure is intentionally generalised.

3.3 Flood Modelling Settings

The modelling framework was designed to simulate the hydraulic response of the study area to extreme precipitation, serving as the driver for PFAS mobilisation and transport. To ensure comparability between the two modelling platforms, the same precipitation statistics were applied to both SCALGO and PluvioFlow.

For this study, the Chicago Design Storm (CDS) method was selected over historical rain events or annual mean data. While historical cloudburst data provides insight into past occurrences, the CDS approach allows for a standardised evaluation of a catchment's response to cloudbursts. Since PluvioFlow utilises the SMHI cloudburst statistics to generate its dynamic CDS hyetographs (SMHI, n.d.-b, 2025), the corresponding total rainfall volumes were manually applied as static inputs in SCALGO to maintain consistency across the simulations (see Table 4). The uncertainty provided by SMHI (Table 4) was not accounted for by either model, and since SCALGO does not allow input with decimals, the 100-year rain amount was rounded up to 54 mm.

Return periods of 10- and 100-years were chosen to represent a range of extreme hydraulic conditions (Table 4). A 10-year event provides a baseline for significant runoff, as this represents the standard design capacity that urban stormwater systems are regulated to handle (MSB, 2023; Svenskt Vatten, 2016). In contrast, the 100-year event represents a more extreme scenario capable of generating large-scale water flows (Svenskt Vatten, 2016). This more extreme scenario is expected to identify transport pathways within the study area that might remain inactive during less frequent 10-year rain events. A duration of 3 hours was selected as a higher middle ground with the idea of achieving a balance between infiltration and runoff processes (Table 4). An extreme rain with shorter duration has the tendency of being too intense for dry soil to infiltrate and most rain will instead migrate as runoff. Conversely, a longer duration typically features a decreased average intensity, giving the soil sufficient time to infiltrate a larger proportion of the rainfall, thereby reducing the fraction that migrates as surface water. To ensure a better representation of the catchment's response, an additional 3 hours were added to the simulation time in PluvioFlow (total of 6 hours). This extended simulation period allows the runoff to continue migrating through the landscape and reaching downstream sinks even after the precipitation has ceased. As mentioned in section 3.2 Study Area, the modelled spatial extent is set to the four surrounding subbasins seen in Figure 2 in section 3.2.1.

Table 4. Cloudburst statistics for the region Southeast Sweden (SÖ). Rain volumes (in mm) for a duration of 3 hours and return periods of 10 and 100 years (Olsson et al., 2017; SMHI, n.d.-b, 2025).

	Return period	
Duration	**10 yrs**	**100 yrs**
3 h	32.0 (± 1.9)	53.5 (± 9.3)

3.4 Identifying Hydrological Patterns

3.4.1 Surface Runoff - Watersheds

To identify the geographic origin of surface runoff contributing to the immediate study area and its potential influence on infiltrated water, a watershed model was developed using the hydrology toolset in ArcGIS Pro (version 3.2.0) (Esri, 2023b). The modelling workflow set up by Esri (2023b) utilised a DEM and began with the Fill tool (no specified Z-limit) to remove depressions and sinks, ensuring continuous flow across the surface. Subsequently, the Flow Direction tool was applied using the D8 method (SFD-algorithm), which assigns flow to the steepest downslope neighbour. The Flow Direction output was used to generate a Flow Accumulation raster, calculating the total upslope contribution to each cell (Esri, 2023b).

To delineate specific surface runoff areas, a polygon feature was utilised to represent the “pour point”, functioning as the system’s hydraulic outlet. In this context, the polygon defines the spatial extent from which contributing upslope flow was backtracked to identify the origin of the runoff.

Given that the DEM contains vertical uncertainties of approximately one decimetre (Lantmäteriet, 2025), a precautionary approach was adopted to account for potential inaccuracies in the DEM. The model was therefore run not only for the immediate study area but also for extended buffer zones of 10, 50, and 100 meters. The immediate study area was digitised in accordance with the fenced-off area where the water treatment plant is located. Finally, the Watershed tool integrated these inputs to delineate the upslope contributing areas, which were then visualised in a map illustrating the spatial extent of the watersheds in relation to the defined buffer zones (see Figure 5 in section 4.1).

3.4.2 Groundwater Recharge Zones

Groundwater recharge zones were identified using the Exceedance Duration tool in PluvioFlow, which quantifies the cumulative time each raster cell maintains a water depth above a user-defined threshold (ranging from 10 cm to 50 cm) throughout the flow simulation (PluvioFlow, 2026a). In this study, the 10 cm depth threshold was selected as the baseline. Areas where the water depth persisted above this threshold for more than 10 minutes were identified as infiltration zones. The choice of a 10-minute threshold was to exclude instantaneous runoff and isolate areas characterised by sustained ponding, which facilitates infiltration. The resulting output is a multi-band raster, where each band represents the time of exceedance for a specific depth. By extracting the data from the 10 cm band that met the 10-minute criteria, potential groundwater recharge zones were delineated. The Exceedance Duration tool served as a proxy for depression focused groundwater recharge areas, since there is a higher likelihood of groundwater recharge in areas susceptible to flooding (Akindele et al., 2024).

3.5 Potential Water Contribution from Land Uses

There are some mismatches between the way SCALGO Live and PluvioFlow operate, therefore some analysis was performed in ArcGIS Pro to achieve a harmonised desired output.

To address the second research question, specific areas of interest were identified based on their potential to contribute to the chemical profile of the infiltrated water. These areas were selected according to two primary criteria. Firstly, the presence of established infiltration zones (as identified in section 3.4.2) and secondly their hydraulic position upstream of the groundwater flow directed toward the infiltration basins in the study area. The selection was geographically constrained to the region north of the southern infiltration basins. As elevated PFAS concentrations were found after the first infiltration and slightly lower after the second infiltration in the south, it was hypothesised that the pollution comes from the direct surroundings of the immediate study area (water treatment plant facility and northern infiltration basins).

The areas of interest were delineated following physical and administrative boundaries, including road networks, watercourses, and property borders. Land use (LU) and specific activities within these delineated zones were identified and then researched further in section 3.6. To ensure spatial consistency across modelling platforms, these LU areas were digitised directly within the PluvioFlow interface and subsequently exported for identical use in ArcGIS Pro.

3.5.1 Surface Runoff and Recharge Zones

Quantitative spatial analysis was performed to determine the extent of surface runoff and infiltration potential within each LU category. The total area of the watersheds (identified in section 3.4.1) that intersect each specific LU area was calculated. This allowed for an assessment of how much surface runoff each LU type potentially contributes to the study area. Similarly, the extent of the infiltration zones (identified in section 3.4.2) falling within each LU boundary was quantified. This step identified which LUs are most likely to facilitate the direct vertical migration of water into the subsurface. These calculations were executed using the Zonal Statistics as Table tool in ArcGIS Pro, specifically the “SUM” statistics. By using the digitised LU polygons as the “zones” and the watershed and recharge zone rasters as the “value” inputs, respectively, a precise area-based summary was generated for each LU area.

3.5.2 Infiltrated Water Volumes – Model Comparison

To evaluate the total volume of water entering the subsurface, two approaches using both models were utilised to compare and validate the results. A dynamic simulation within the PluvioFlow environment and a static spatial analysis reconstructed in ArcGIS Pro based on SCALGO’s infiltration methodology.

3.5.2.1 PluvioFlow Methodology

The PluvioFlow simulation employs a two-phase infiltration model to characterise the soil's absorption capacity over time (PluvioFlow, 2026b). Each cell is assigned a pre-infiltration capacity representing dry soil conditions and a lower post-infiltration rate for saturated conditions (PluvioFlow, 2026b). According to the model parameters, once ~ 90 % of the soil's water storage capacity is reached, the infiltration rate diminishes to ~ 10 % of the initial rate (PluvioFlow, 2026b). The primary metric extracted from this simulation was the Accumulated Infiltration Depth, a cumulative time-series raster recorded in millimetres (mm) (PluvioFlow, 2026a). This layer represents the total rainfall absorbed by the soil up until a chosen time step (PluvioFlow, 2026a). In this study, the last time step (3h) was chosen to get the accumulated infiltration depth for the entire simulation. To determine the volumetric contribution per LU category, area samples were performed within the PluvioFlow interface for each digitised LU polygon. The software calculated the total volume in m^3 by integrating the accumulated depth across the specific cell count of each LU area.

3.5.2.2 SCALGO-Based Static Modelling in ArcGIS Pro

Because SCALGO and PluvioFlow utilise different interfaces and provide different formats of output, a comparative analysis was performed in ArcGIS Pro by replicating SCALGO Live's infiltration logic. SCALGO's method determines infiltration by the surface compaction, which is assessed based on the land cover class (*Land Cover* layer in SCALGO), as well as the soil typology *(Topsoil type* layer in SCALGO) in natural areas and sewer map status (*Tätorter layer* in SCALGO) in artificial areas (SCALGO, n.d.-b). Since the study area is located outside the urban area boundaries (*Tätorter* layer in SCALGO), the model makes the assumption that artificial surfaces lacked sewer systems, and therefore all rainfall on these surfaces becomes runoff (SCALGO, 2024). The infiltration in natural areas is determined by a runoff calculation based on rainfall intensity (CDS) and the soil's infiltration capacity (Horton's equation) of high and low compaction grade, respectively (SCALGO, 2024).

SCALGO generate its own topsoil and land cover data based on available knowledge (SCALGO, 2024). The process begins with the synthesis of nationwide coverage using superficial deposits data (*jordartsdata*) from the Geological Survey of Sweden (SGU), see Table 3 (SCALGO, n.d.-b). SCALGO prioritises high-resolution SGU datasets, such as the 1:25,000 to 1:100,000 layers, to define the soil types and utilises coarser regional maps to ensure seamless national coverage (SCALGO, n.d.-b). These SGU typologies are subsequently mapped to a Scandinavian-specific soil typology based on the Danish JB (*jordbundstyper*) classification system (SCALGO, n.d.-b, n.d.-e). To create the Topsoil layer, SCALGO characterises soils primarily by fractions of fine sand, sand, silt and clay in accordance with the JB system, while adding supplemental classes for non-soil features like bedrock, gravel, and water. SCALGO's Land Cover map is produced based on machine learning techniques, orthophotos and other input data (hydrography, buildings, roads, railroads and agricultural blocks, see section 3.1 Data) at a resolution of 25 cm (SCALGO, n.d.-b, n.d.-d). More specifically, how these datasets are used to produce the Land Cover map is insufficiently documented.

The Topsoil and Land Cover layers generated by SCALGO was uploaded to ArcGIS Pro for further re-creation of the SCALGO infiltration methodology. Initially, the SCALGO Land Cover layer was reclassified into four distinct compaction degrees (Table 5). Simultaneously, the Topsoil layer was utilised to identify soil typologies, ranging from high-permeability gravel to low-permeability clay (Table 6). These two variables were summarised using the Raster Calculator tool to generate unique integer values. In this classification scheme, the hundredth digit represented the compaction state, while the subsequent digits identified the soil type (e.g., a value of 102 representing "High Compaction" on "Gravel").

Table 5: Reclassification of landcover to compaction degrees.

Compaction degree	Assigned value	Original landcover classes
High	100	Unpaved road, Bare land, Shallow vegetation, Field, Bare rock, Railroad
Low	200	Dense vegetation
Artificial	300	Building, Paved road, Other paved
Glass/Water	400	Water

Table 6: Soil type and assigned values.

Soil type	Assigned value by SCALGO
Gravel	2
Coarse sand	3
Fine sand	4
Fine sand with clay	6
Course clay with sand	7
Fine clay with sand	8
Clay	9
Fine clay	10
Gyttja/peat	13
Bedrock	14
Water	16

These unique combinations were then mapped to the corresponding runoff function in SCALGO. A water balance approach was then adopted, excluding evaporation. All rainfall not accounted for by the runoff functions was therefore treated as infiltrated depth, i.e. the infiltrated depth per pixel was calculated by subtracting the modelled runoff from the total rainfall for both 10-year and 100-year return periods (SCALGO, 2024). Consequently, neither evaporation nor evapotranspiration was accounted for.

The resulting rasters, with a spatial resolution of 1x1 meters, provided the infiltrated depth in meters for a 10-year respectively a 100-year rain event. To calculate the final volume per LU, the Zonal Statistics as Table tool was applied using the SUM statistic. By aggregating the depth values of all pixels within each digitised LU zone, a volumetric summary was generated, allowing for a direct comparison with the PluvioFlow results.

3.6 Land Use Related PFAS Usage – Literature Study

Initial identification of suspected and confirmed polluted areas was performed using *EBH-stödet* and the associated *EBH-kartan*, a national database managed by the County administrative boards of Sweden that maps and monitors contaminated sites (Länsstyrelserna, 2025). These locations were further verified against the register for environmentally hazardous activities, also managed by the County administrative boards of Sweden, to determine their regulatory status and industry classification activities (Länsstyrelsen Södermanlands län, n.d.; Länsstyrelserna, 2020). To supplement the official records, spatial observations were conducted using Google Maps and the business registry provided by the Swedish Companies Registration Office *Bolagsverket* (Bolagsverket, n.d.; Google, n.d.-a). This allowed for the identification of small-to-medium enterprises (SMEs) and specific land-use activities, which may not be formally registered in national pollution databases but may be relevant to the usage of PFAS.

All identified industrial classes and LU activities were cross-referenced with the Swedish Environmental Protection Agency's (*Naturvårdverket* - NVV) Industry List (NVV, 2025a). This reference serves as a standard for identifying industry-specific and industry-related PFAS pollution based on established literature and historical usage patterns. NVV categorised industries by their BKL (*Branschklassning*) to assess their potential contribution to ground and sediment contamination.

For LU categories and activities not explicitly detailed in the NVV Industry List (NVV, 2025a), a targeted literature review was performed. The search focused on publications and reports from the Swedish Chemicals Agency (*Kemikalieinspektionen* - KEMI), the Swedish Environmental Protection Agency (*Naturvårdverket* - NVV) and the Swedish Board of Agriculture (*Jordbruksverket*). These documents and websites were found using keywords in Swedish, including "PFAS", "Agriculture", "Agricultural field" and "Household". The search was supplemented using the snowball method. The search for scientific peer-reviewed literature was made using the bibliographic database "Science Direct" with the keywords (PFAS) AND (agriculture) AND (leaching) AND (Sweden) and with the filters article type: Research article and Access type: Open access & Open archive. The first selection was made based on titles with thematic relevance, while the second selection was made after reviewing the abstract and conclusion for relevance. Also in this step, the snowball method was utilised. Primary sources were primarily used. When secondary sources were used, they were critically reviewed and assessed as reliable in order to maintain the study's credibility.

4 Result

4.1 Spatial Patterns of Watersheds and Recharge Zones

The hydrological watershed modelling successfully identified the upslope contributing areas for the immediate study area and its surrounding buffer zones (Figure 5). The spatial extent of the calculated watersheds from the immediate area to the 50 m buffer reveals a drainage basin located primarily to the southeast of the water treatment plant. As the analysis moved from the immediate area to the 10 m and 50 m buffer zones, the identified watershed area expanded slightly. While the “Immediate”, “10 m” and “50 m” watersheds are localised primarily to the site’s southeastern boundary, the “100 m” watershed captures a massive catchment area extending approximately 8 kilometres to the southwest. This large increase is likely due to the 100 m buffer zone intersecting the ditch to the west of the immediate study area, acting as a major flow accumulation path (Figure 5). Consequently, the 100 m watershed provides the most comprehensive “worst-case” boundary for identifying potential upstream sources of infiltrated water or chemical contaminants.

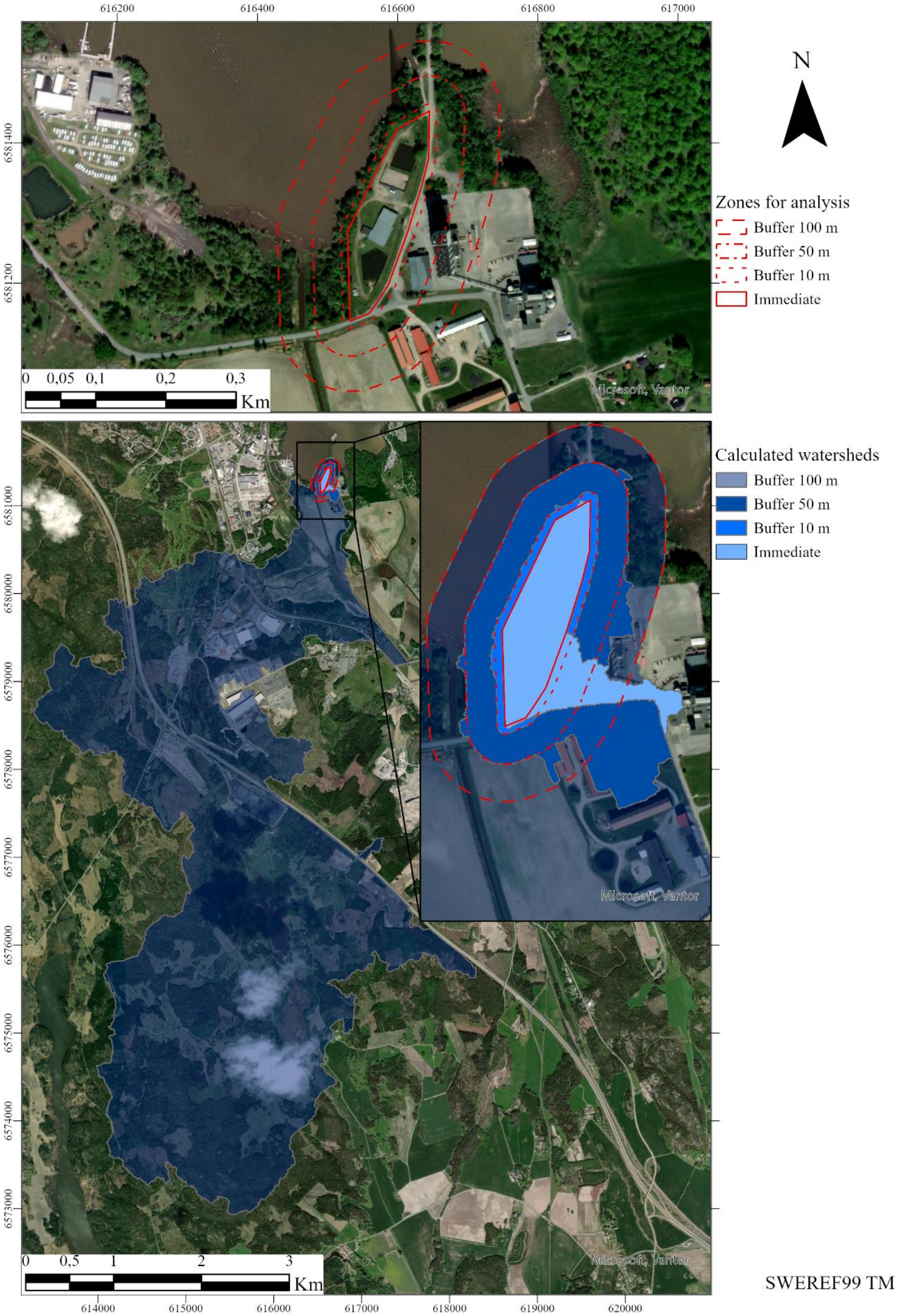

Figure 5. Calculated watersheds from different buffer zones and the immediate study area around the water treatment plant. The watersheds represent surface runoff pathways. A calculated watershed includes the area of any smaller watershed. Basemap: World Imagery [1]

The mapping of exceedance durations illustrates the spatial distribution of potential groundwater recharge zones under two precipitation scenarios (Figure 6). These zones are non-uniformly distributed, with concentrations primarily located within topographical depressions and along drainage corridors, such as agricultural ditches and low-lying areas within fields. In the 10-year rain event, the recharge zones are largely fragmented, consisting of isolated "islands" of ponding within the deepest topographical lows. These areas represent the most consistent sites for vertical water migration across both scenarios. During the 100-year rain event, the spatial extent expands to encompass these 10-year zones while largely increasing the total area of active infiltration, especially the footprint on fields (Figure 6). This expansion merges previously isolated zones into larger, continuous areas of ponded water and increases the overall spatial diversity of the surfaces through which water enters the subsurface. While the 10-year extent identifies the primary points of infiltration, the 100-year extent reveals the larger potential spatial reach of the recharge process across the study area.

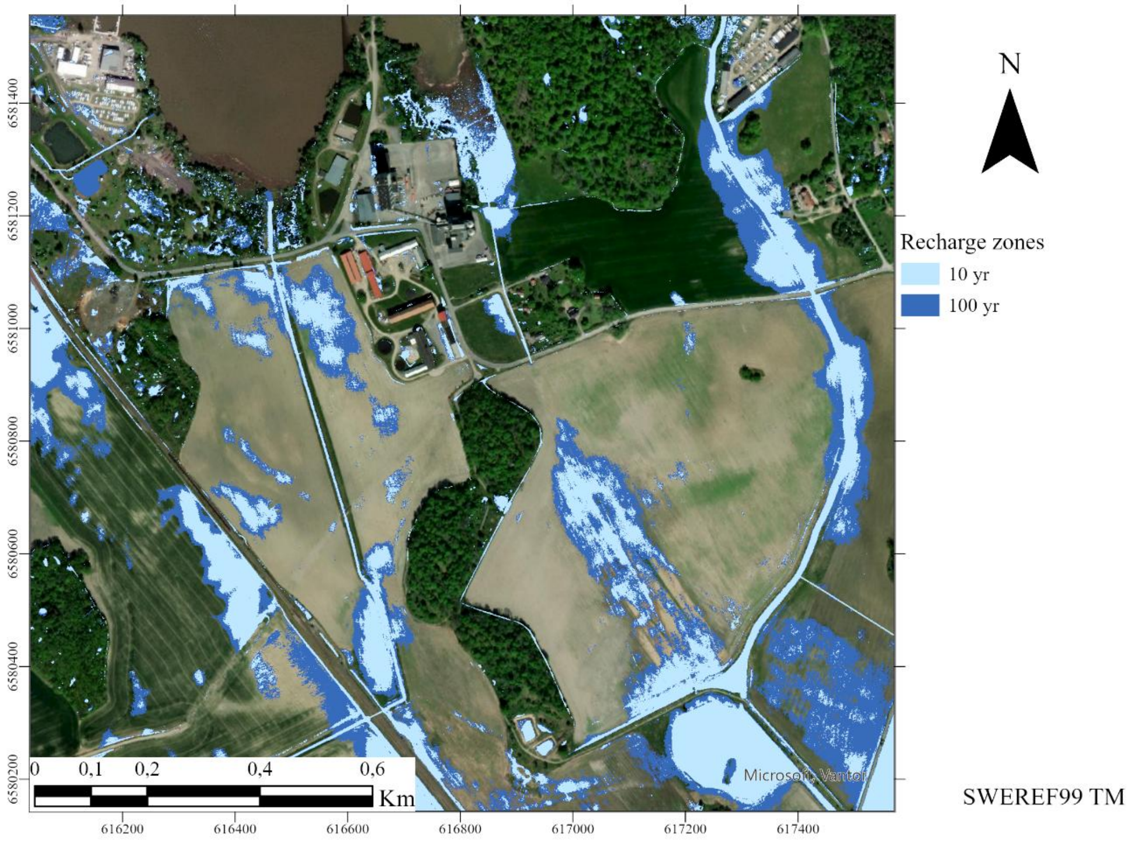

Figure 6. Map visualising the spatial distribution of the groundwater recharge zones identified with PluvioFlow's exceedance duration tool (threshold 10 cm). The recharge zones present during a 10-year rain event are also included in a 100-year rain event. Basemap: World Imagery [1]

4.2 Potential Water Contributions from Land Uses

The delineation of land use (LU) zones within the area of interest resulted in the identification of six distinct areas, labelled A through F (Figure 7). The identified LU zones represent four primary land use categories: cereal industry (F), farmsteads/SME (D), households (B) and agricultural fields (A, C and E). An SME is a Small-Medium Enterprise as defined by the European Commission (Commission Recommendation of 6 May 2003 Concerning the

Definition of Micro, Small and Medium-Sized Enterprises, 2003). Table 7 shows that agricultural fields (A, C and E) together constitute the largest portion of the investigated area, even though Zone C present the smallest area on its own. Households (B) have the next to smallest presence to the southeast of the study area. The cereal industry (F) and farmstead/SME (D) zones are situated in closer proximity to the water treatment plant's immediate surroundings. These six polygons (A–F) serve as the spatial units for the subsequent quantitative analysis of surface runoff and recharge areas, as well as infiltration volumes.

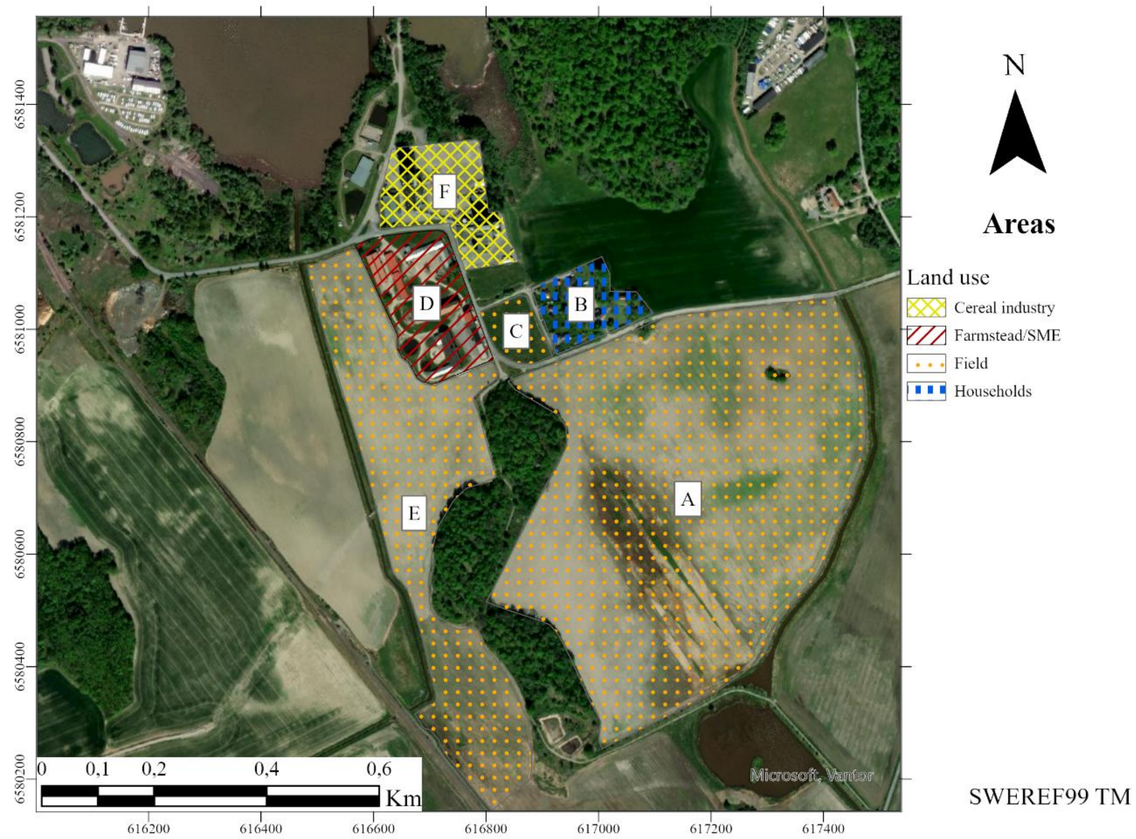

Figure 7. Map visualising the identified land uses within a proximity of interest of the study area. Each individual land use zone is labelled with a letter A-F. Basemap: World Imagery [1]

Table 7. Presentation of the areas (in hectares ha) of the land use zone (A-F) visualised in Figure 7.

	A	B	C	D	E	F	All fields (A+C+E)
Area (*ha*)	34.60	1.97	1.00	3.95	13.14	3.36	48.73

4.2.1 Surface Runoff - Watersheds

The intersection of the calculated watersheds and the six LU zones reveal an increase in areal overlap, as the analysis area (buffer zones) around the study site increases (Figure 8). The quantitative distribution of these overlapping areas, summarised in Table 8, highlights which land uses contribute surface runoff to the various buffer zones. At the highest level of proximity, surface runoff contribution is exclusively limited to the closest 200 m in the east-to-southeast direction from the study area.

Both the Immediate and 10 m buffer watersheds intersect only with LU Zone F (cereal industry), with overlapping areas of 0.55 and 0.58 ha, respectively. No other LU zones contribute to the surface drainage at these scales, indicating that the immediate hydraulic environment of the water treatment plant is primarily influenced by the cereal industry.

The 50 m buffer watershed marks a transition in hydrological connectivity, as it begins to incorporate a wider variety of anthropogenic activities. While Zone F remains a contributor (1.13 ha), the watershed expands southwards to include a significant portion of Zone D (farmstead/SME) at 1.50 ha and a smaller section of Zone E (field) at 0.27 ha. As seen in Figure 5 this shift at a 50-meter margin, suggests the potential runoff catchment begins to move beyond the industrial Zone F into both the agricultural Zone E and the farmstead/SME Zone D.

The 100 m buffer watershed represents the most extensive hydrological link, showing a massive increase in total contributing area. The most significant spatial contribution comes from Zone E (field), which accounts for 12.35 ha of the overlap a forty-fold increase from the 50 m scenario. This is followed by Zone D (farmstead/SME) at 3.98 ha. While Zone F's contribution increases to 1.56 ha, it becomes a secondary contributor relative to the vast agricultural and farmstead/SME areas identified to the south.

Notably, Zones A, B, and C (comprising households and eastern agricultural fields) show zero overlap across all watershed scenarios, indicating that despite their proximity, they remain hydrologically disconnected from the surface runoff pathways directed toward the study site.

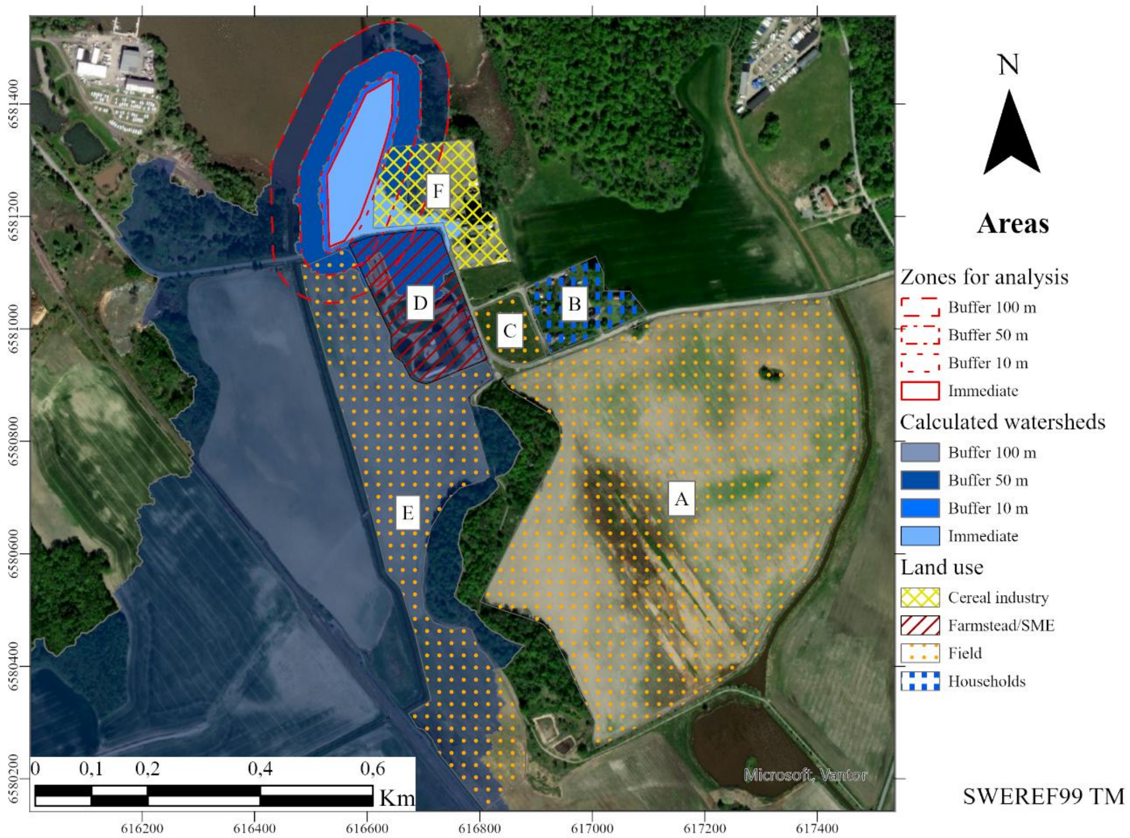

Figure 8. Map visualising the areal overlap between the calculated watersheds and the land use zones. Basemap: World Imagery [1]

Table 8. Presentation of the overlapping areas (in hectares, ha) between watersheds and land use zones (seen in Figure 8). A calculated watershed includes the area of the smaller ones.

Calculated watersheds	A	B	C	D	E	F
Immediate watershed	0	0	0	0	0	0.55
Buffer 10 m	0	0	0	0	0	0.58
Buffer 50 m	0	0	0	1.50	0.27	1.13
Buffer 100 m	0	0	0	3.98	12.35	1.56

4.2.2 Recharge Zones

The intersection of the modelled recharge zones and the identified LU zones shows that potential vertical infiltration is predominantly concentrated within the agricultural fields in the study area (Figure 9). Table 9 quantifies these overlapping areas, showing a significant increase in the infiltration footprint across all identified land uses when moving from a 10-year to a 100-year rain event.

Agricultural fields (A and E) constitute the majority of the total recharge area in both precipitation scenarios. In the 10-year event, Zone A and Zone E account for 2.75 and 1.22 ha of active recharge areas, respectively. These areas more than double during the 100-year event, with Zone A expanding to 6.43 ha and Zone E to 3.14 ha. The third field (C) also shows a large increase, rising from 0.12 to 0.21 ha, nearly a doubling in areal extent. Despite its smaller dimensions compared to Zones A and E, Zone C shows a great proportional extent of recharge area relative to its total size (Figure 9). This spatial concentration indicates that the primary pathways for groundwater recharge in the study area are located in open fields, particularly in topographic depressions visible in Figure 9.

While smaller in absolute area, the industrial and household zones (B, D, and F) also show consistent recharge activity. Zone D (farmstead/SME) exhibits a notable recharge footprint, increasing from 0.18 ha in the 10-year event to 0.30 ha in the 100-year scenario. In contrast, the cereal industry (F) and households (B) show the smallest relative overlap. Zone F exhibits a recharge area of 0.06 ha (10-yr), which increases to 0.13 ha (100-yr), while Zone B remains the most hydrologically isolated at only 0.02 ha (10-yr) and 0.03 ha (100-yr). The mapping in Figure 9 demonstrates that the more extreme 100-year event not only expands existing recharge zones in a 10-year event but also increases their geographic diversity.

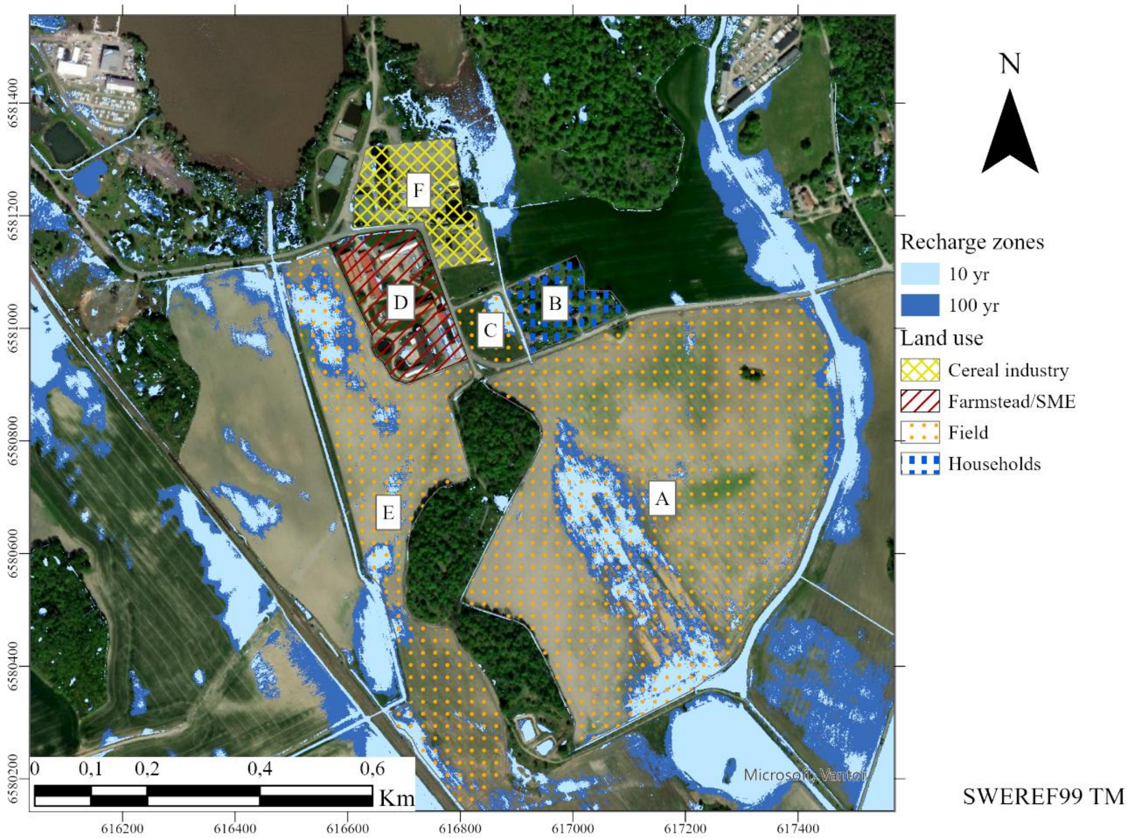

Figure 9. Map visualising the areal overlap between the groundwater recharge zones and the land use zones. Basemap: World Imagery [1]

Table 9. Presentation of the overlapping areas (in m^2) between groundwater recharge zones and land use zones (seen in Figure 9). The 100-yr recharge zones include the area of the 10-yr recharge zones.

	A	B	C	D	E	F
10 yr	2.75	0.02	0.12	0.18	1.22	0.06
100 yr	6.43	0.03	0.21	0.30	3.14	0.13

4.2.3 Comparative Volumetric Infiltration Analysis

The volumetric analysis of infiltrated water across the identified LU zones highlights the agricultural fields as substantial contributors, while the "Average Per Pixel" metrics reveal the intensity of infiltration regardless of zone size (Table 10). By comparing these values, a distinction can be made between zones that contribute high volumes due to their large spatial extent and zones that exhibit high infiltration intensity due to local surface characteristics.

The agricultural fields account for the vast majority of total infiltrated volume in both rain events and models, driven largely by the significant spatial extent of Zones A and E. Additionally, the infiltration per pixel differs only by up to 0.4 mm between these zones under both rain scenarios and for both models. Zone A and E also present percent differences relatively close to 0 for both rain events, with PluvioFlow estimating slightly higher (+8.8 and +11.3, respectively) for the 10-year event and a slight lower (-5.4 and -4.0, respectively) for the 100-year event compared to SCALGO. In contrast, Zone C, is estimated to contribute the least total infiltration volumes according to PluvioFlow and next to lowest volumes according to

SCALGO. In contrast to the other fields, estimated SCALGO higher infiltration intensities (15.1 and 18.1 mm under respectively rain event), while PluvioFlow estimated more similar as to the other fields (10.4 and 11.3 under respectively rain event). In this field (Zone C), the models exhibit substantially larger differences in their results, as the percent difference ranges from -30.8 to -37.8 % under respective rain events (Table 10). Table 11 presents the combined data for the three agricultural fields (Zones A, C, and E). These zones demonstrate the highest level of model convergence (percent difference close to 0), with an average percent difference of less than ± 10% between the two models (Table 11). In the 10-year event, PluvioFlow estimated a total agricultural infiltration volume of 5,603.4 m³, which is 8.4 % higher than SCALGO's estimation of 5,171.2 m³. This is also reflected in the average infiltration per pixel, where PluvioFlow recorded 11.5 mm compared to SCALGO's 10.6 mm. However, during the 100-year event, the relationship is reversed, where SCALGO's total volume of 6,435.4 m³ exceeds PluvioFlow's 6,056.5 m³ by 5.9 %. This trend indicates that while both models show increased infiltration with increased precipitation, they do so at slightly different rates. PluvioFlow's average infiltration per pixel shows a smaller relative increase between the two return periods (11.5 to 12.4 mm) compared to SCALGO's shift (10.6 to 13.2 mm), see Table 11. Ultimately, due to the vast spatial extent of these zones, they remain the primary geographic contributors to groundwater recharge regardless of which modelling platform was used.

Similarities and divergences between SCALGO and PluvioFlow are also observed in the built-up LU zones (B, D and F). Zone B (households) and Zone D (farmstead/SME) show the highest average infiltration per pixel in the SCALGO model, at 27.0 mm (B) and 20.5 mm (D), respectively, during the 100-year event (Table 10). PluvioFlow, however, estimates 48.2 % (B) and 44.6 % (D) lower infiltration for the 10-year rain event and 58.5% lower for these same zones in the 100-year scenario. Conversely, Zone F (Cereal Industry) is the only area where PluvioFlow consistently estimates higher intensity than SCALGO. Zone F exhibit the lowest total infiltration volumes according to SCALGO and next to lowest according to PluvioFlow, but both models agree that Zone F exhibit the lowest infiltration intensity. In the 10-year event, PluvioFlow's per-pixel average is 62.7 % higher compared to SCALGO (5.7 and 3.5 mm, respectively), and in the 100-year event 22.5 % higher (5.9 and 4.8 mm, respectively) (Table 10).

Table 10. Presentation of total volume of infiltrated water and average infiltration volume per pixel within each land use zone (Figure 7) for 10- and 100-year rain calculated by SCALGO and PluvioFlow, respectively. Total volumes are presented in the unit m^3, and the average infiltration per pixel is given as an infiltration depth in mm, where the pixel size is 1x1 m (i.e. mm/m^2). The percent difference (in %) shows how PluvioFlow compares to SCALGO.

	Metrics	A	B	C	D	E	F
10 yr	SCALGO (*m^3*)	3640.2	399.5	150.6	577.8	1380.4	117.8
	PluvioFlow (*m^3*)	3962.3	206.9	104.2	319.9	1536.9	191.6
	SCALGO avg. per pixel (*mm/m^2*)	10.5	20.2	15.1	14.6	10.5	3.5
	PluvioFlow avg. per pixel (*mm/m^2*)	11.5	10.5	10.4	8.1	11.7	5.7
	Percent Difference (%)	+8.8	-48.2	-30.8	-44.6	+11.3	+62.7
100 yr	SCALGO (*m^3*)	4512.4	532.4	180.7	811.4	1742.3	162.4
	PluvioFlow (*m^3*)	4270.9	220.8	112.4	336.4	1673.2	199.0
	SCALGO avg. per pixel (*mm/m^2*)	13.0	27.0	18.1	20.5	13.3	4.8
	PluvioFlow avg. per pixel (*mm/m^2*)	12.3	11.2	11.3	8.5	12.7	5.9
	Percent Difference (%)	-5.4	-58.5	-37.8	-58.5	-4.0	+22.5

Table 11. Summary of infiltration results over all agricultural fields (zones A, C and E) for 10- and 100-year rain calculated by SCALGO and PluvioFlow, respectively. Total volumes are presented in the unit m^3, and the average infiltration per pixel is given as an infiltration depth in mm, where the pixel size is 1x1 m (i.e. mm/m^2). The percent difference (in %) shows how PluvioFlow compares to SCALGO.

	10 yr	**100 yr**
SCALGO Total Volume	5,171.2	6,435.4
PluvioFlow Total Volume	5,603.4	6,056.5
SCALGO avg. per pixel	10.6	13.2
PluvioFlow avg. per pixel	11.5	12.4
Percent Difference (%)	+8.4	-5.9

4.3 PFAS Usage Associated with Land Uses

Analysis of the Swedish national database for *suspected* or *confirmed* polluted areas (EBH-stödet) revealed no *confirmed* contaminated sites within the LU zones identified in section 4.2 (Länsstyrelserna, 2025). However, four sites of interest were identified based on their industrial classifications (Table 12). The nearest *confirmed* polluted area is located at Gorsinge harbour, situated on the cape north of the study area, and is part of the industry class "Harbour – Trade traffic with environmentally hazardous goods" (Länsstyrelserna, 2025). However, there were three *suspected* polluted areas, one located on the water treatment plant, i.e. the immediate study area, and two in the LU Zone F (cereal industry), see Table 12. The water treatment plant and the northwestern building in Zone F both belong to the industry class "Other BKL 4", i.e. objects not fitting under any other industry class but are considered low risk (Länsstyrelserna, 2025; NVV, 2025a). In contrast, the southeastern building in Zone F is classified under "Treatment of grain" (Länsstyrelserna, 2025), and is formally registered as an environmentally hazardous activity (Länsstyrelsen Södermanlands län, n.d.; Länsstyrelserna, 2020) .

Table 12. Suspected or confirmed polluted areas according to EBH-stödet (Länsstyrelserna, 2025).

Location	Status	Industry class	ID (EBH-stödet)
Gorsinge harbour (outside LU zones)	Confirmed	Harbour – Trade traffic with environmentally hazardous goods	133733
Water treatment plant (Immediate study area)	Suspected	Other BKL 4	133548
F (Cereal industry) Northwest building	Suspected	Other BKL 4	133524
F (Cereal industry) Southeast building	Suspected	Treatment of grain	183929

To evaluate the potential for PFAS contamination, the identified industrial activities in Table 12 were cross-referenced with the NVVs Industrial list (NVV, 2025a). This list identifies potential PFAS usage and industry-related pollution based on established literature (NVV, 2025a), and the findings of interest from this list are presented in Table 13.

The Gorsinge harbour, despite being outside the LU zones, is a notable potential source, as its classification is linked to industry-related PFAS pollution in sediment and potential ground contamination, see Table 13 (NVV, 2025a). As presented in Table 13 the water treatment plant and the northwestern building in Zone F, identified as industry class "Other BKL 4", are not categorised as industries using PFAS (NVV, 2025a). Consequently, no definitive conclusion regarding PFAS usage can be drawn for these locations without further research. However, the southeastern building in Zone F ("Treatment of grain") is categorised as a potential PFAS industry associated with ground pollution and a potential user of pesticides, see Table 13 (NVV, 2025a).

Beyond the EBH-stödet database, additional potential sources were identified through land-use and activity observations in Google Maps. In LU Zone D (farmstead/SME), a car and boat storage facility with an associated garage was identified (Google, n.d.-b; Strängnäs Båt & Bilförvaring, n.d.). The car and boat storage facility were however not found as an active or inactive registered company at the Swedish Companies Registration Office (Bolagsverket, n.d.) and is therefore hard to legitimise its existence. While not registered as a polluted area or an environmentally hazardous activity, these operations align with the industry classes “Car care facility” and “Harbour – Recreational boat harbour/storage” (Länsstyrelsen Södermanlands län, n.d.; Länsstyrelserna, 2020, 2025). According to the NVVs Industry list, car care facilities are associated with industry-related PFAS pollution in soil, while recreational boat storage is linked to PFAS in both sediment and ground, see Table 13 (NVV, 2025a).

Table 13. Industry-specific and industry-related PFAS usage (NVV, 2025a).

Industry class	BKL	Industry-specific or -related PFAS pollution	Comment
Identified with EBH			
Harbour – Trade traffic with environmentally hazardous goods	2	PFAS in sediment (related)	Potential PFAS industry, Ground pollution
Other BKL 4	4	-	Site specific
Treatment of grain	2	-	Potential usage of pesticides Potential PFAS industry, Ground pollution
Other identified activity			
Car care facility	3	PFAS in ground (related)	
Harbour – Recreational boat harbour/storage	2	PFAS in sediment (related)	Potential PFAS industry, Ground pollution

The LUs agricultural fields (Zones A, C, and E) and households (B) are not stated in the NVV Industy list. Despite their absence from this formal industrial register, literature suggests connections of varying significance between these LUs and PFAS.

Globally, the most extensively examined sources of PFAS into agricultural soils are the application of biosolids (sewage sludge) and the use of contaminated irrigation water, both of which are byproducts or direct products of wastewater treatment plants, as well as pesticides (Biswas et al., 2025; Ghisi et al., 2019). In Sweden, the use of treated sewage sludge as fertilizer is a documented pathway for PFAS into agricultural land (NVV, 2025b). A report from Kärrman et al. has shown that sludge serves as a distribution pathway for PFAS to arable land, as a clear correlation exists between increased application rates and higher PFAS concentrations in the soil, and that its accumulation can impact both ground and surface water bodies, contributing to long-term PFAS leakage from agricultural areas (Kärrman et al., 2024). Consequently, the application of sludge to agricultural lands represents a significant exposure pathway for PFAS to both humans and the environment (Fredriksson et al., 2022; Lindstrom et al., 2011). When it comes to pesticides, there are currently 18 active PFAS substances used in approved plant protection products in Sweden, and 11 more in the EU (KEMI, 2026a). Additionally, six active substances defined as PFAS are approved for use in biocidal products within the EU, with three of these substances currently used in approved products in Sweden (KEMI, 2025). Some PFAS-based pesticides/biocides/herbicides can degrade into trifluoroacetic acid (TFA), a highly mobile ultra-short-chain PFAS (Naturskyddsföreningen, 2024). Potatoes are a major Swedish crop that is heavily dependent on chemical plant protection to manage potato blight (*potatisbladmögel*) (A. Andersson et al., n.d.). Among the active substances approved for use in Swedish potato cultivation, eight are classified as PFAS substances that can form TFA (A. Andersson et al., n.d.). In the Swedish agricultural landscape, the occurrence of TFA is particularly high compared to other land uses (Boström et al., 2024). Measured concentrations range between 890-2,400 ng/L in running water and have been found as high as 5,400 ng/L in groundwater (Naturskyddsföreningen, 2024). Among the PFAS-classified herbicides that can form TFA, identified by The Swedish Chemicals Agency, diflufenikan (DFF) and pyroxsulam are the most widely used in Sweden (Lundkvist et al., n.d.). When it comes to PFAS uptake in plants, (Ghisi et al., 2019) found that polluted water and biosolids also act as the primary source in this case. This is particularly relevant for LU Zone F (Cereal industry), as the leaves of cereals and vegetables have been found to accumulate high levels of short-chain PFAS (Ghisi et al., 2019).

While no significant direct connections were identified between PFAS pollution and households (Zone B) in the literature, it was found that households act as secondary sources of diffuse emissions through the use and degradation of consumer products. Common items found in Swedish households that contain PFAS include grease-resistant food packaging, non-stick cookware, stain-resistant textiles such as carpets and furniture, and various cosmetics (KEMI, 2026b). These treated products contribute to the accumulation of PFAS in the indoor environment. Consequently, high concentrations are often found in indoor dust and air within Swedish homes (NVV, 2025b). However, it does not state the effect of this indoor dust on the direct outside environment. The release of these chemicals into the water cycle may occur through domestic activities, such as laundering water-resistant clothing (e.g., Gore-Tex) or the use of PFAS-containing cleaning agents (KEMI, 2024b). It is important to note that if households are connected to municipal sewage systems, these pollutants are transported to wastewater treatment plants rather than leaching directly into the immediate environment surrounding the home. No basis for whether the households in Zone B are connected to municipal sewage systems could be provided by the municipality. However, as previously noted, PFAS in household products may eventually concentrate in sewage sludge, which may then be recirculated into the environment via agricultural application.

5 Discussion

5.1 Results Discussion

5.1.1 Hydrological Dynamics and Infiltration Analysis

A primary finding is the dominance of Zone F (cereal industry) for surface runoff remaining hydrologically connected across all watershed scales (Figure 8 and Table 8), suggesting that any surface contaminants here have a direct pathway with surface runoff to the water treatment plant's immediate vicinity. The watershed analysis however only exhibits where runoff may originate, not the volume of runoff. Consequently, Zone F also exhibit among the lowest total infiltration volumes as well as the lowest average infiltration per pixel depths (Table 10). The low average infiltration per pixel suggests the zone is dominated by impervious surfaces, and that most rainfall which lands here is redirected as surface runoff. This idea that Zone F mostly create surface runoff, in combination with the results of the watershed analysis, showing consistent runoff connectivity to the study area, concludes that Zone F may be a primary contributor of surface runoff.

A "worst-case" finding for surface runoff occurs when the watershed analysis is applied to the 100 m buffer zone, where the calculated watershed expands to approximately 8 km in the southwest direction from the immediate study area (Figure 8). While this expansion identifies the additional contribution of surface runoff from Zone D and E, the 8 km watershed also encompasses a vast area of upstream land uses not captured in this specific LU analysis, since the main focus in this report is on what may happen between the two PFAS measuring points in the north and south (see Figure 4). However, this significant enlargement of the watershed may be due to the 100 m buffer zone intersecting a major drainage ditch, suggesting runoff from this watershed may pass through this ditch next to the study area and out into Mälaren.

Interestingly, despite their proximity to the treatment plant, Zone B (households) and the eastern fields (Zones A and C) remain hydrologically disconnected from the site via surface runoff (Figure 8), effectively ruling them out as primary surface-flow contributors.

When analysing infiltration behaviour, a clear distinction emerges between the total volume and the intensity. While Zones A and E (agricultural fields) exhibit the largest total infiltration volumes (Table 10), looking at the average infiltration per pixel, both zones demonstrate highly comparable infiltration intensities with each other and Zone C (field). It can therefore be concluded that the large total infiltration volume is largely a function of Zone A and E's significant spatial extent (Figure 7). The similar infiltration intensity between these two fields diverges from the third small field (Zone C), where the model estimations diverge slightly more than for the large fields (A and E). The infiltration intensities are however similar enough between all fields to suggest that also Zone C's small total volumetric contribution may be driven by its size (Table 7). In relation to its small area, Zone C exhibit a relatively large recharge area under both rain events (Figure 9 and Table 9), suggesting a hotspot for ponding and groundwater recharge.

Similarly, the built-up Zones B and D (households, respectively farmstead/SME) demonstrate mid to high per-pixel intensity, indicating that while their total volumetric infiltration is lower, they contain higher permeable surfaces where the rate at which surface water flushes through these zones is higher (Table 10). The divergence between the model estimations is quite large, up to 58.5 % (Table 10), making it difficult to conclude these zones true permeability. Additionally, the continuously lower estimations which PluvioFlow makes (Table 10) for these two LU zones suggest that while SCALGO identifies these built-up zones as high-intensity infiltration points, PluvioFlow's dynamic simulation possibly routes more water away as surface runoff, leading to SCALGO presenting comparably higher localised infiltration depths.

5.1.2 Evaluation of Potential PFAS Sources

By synthesising land-use activities and potential PFAS usage with hydrological pathways, several high-priority source areas emerge.

When investigating industry-related PFAS usage, Zone F (cereal industry) stands out as a critical area of interest, since the southeastern building is categorised as a "Treatment of grain" industry, associated with both potential PFAS ground pollution and potential pesticide usage (Table 13). Given its direct surface runoff connection to the water treatment plant (Figure 8), it represents a high-probability source for short-chain PFAS, which have been shown to accumulate in the leaves of cereal crops via agricultural chemicals (Ghisi et al., 2019).

Since the water treatment plant and the northwestern building in Zone F were identified as "Other BKL 4" they pose low pollution risk. However, the activity is undefined and no definitive conclusion regarding PFAS usage can be drawn for these locations without further research. PFAS pollution could arise in the water treatment plant itself from e.g. pipes or filter membranes which may contain PFAS (Glüge et al., 2020).

Zone D (farmstead/SME) presents a localised risk through its boat and car storage facility. While unregistered in official databases for suspected polluted areas, its land use aligns with categories associated with PFAS pollution in soil and sediment. However, it is important to note that since this activity is not registered as an active or inactive business at the Swedish Companies Registration Office *Bolagsverket* it is hard to draw any conclusions on the extent of this activity. As mentioned above (section 5.1.1), the SCALGO modelling indicates that Zone D possesses some of the highest infiltration intensities (14.6 to 20.5 mm per pixel), suggesting an efficient infiltration of potentially polluted water, while PluvioFlow's estimations are lower. Additionally, Table 9 indicated quite large recharge areas where this potentially polluted water may infiltrate. However, depending on the groundwater flow direction the infiltrated water may or may not reach the water treatment plant, regardless of which modelled infiltration intensity is most realistic.

Finally, when combining the hydrological analysis with literature findings agricultural fields (A, C and E) stand out as massive potential diffuse sources of PFAS pollution to the groundwater (and runoff for Zone E). The literature presented in section 4.3 suggests these agricultural fields may act as a long-term reservoir for PFAS due to the potential application of sewage sludge and the use of TFA-forming pesticides (A. Andersson et al., n.d.; Biswas et al., 2025; Boström et al., 2024; Ghisi et al., 2019; Kärrman et al., 2024; KEMI, 2025, 2026a; Lundkvist et al., n.d.; Naturskyddsföreningen, 2024). The sheer volume of water moving through the fields A, C and E combined (over 5,000 m^3 in a 10-year event and 6,000 m^3 in a 100-year event) could facilitate large amounts of diffuse leaching into the groundwater (Table 11).

5.1.4 Flow Uncertainties

The interpretation of these sources when it comes to potential groundwater pollution is ultimately constrained by the local groundwater dynamics. As mentioned in section 3.2.3, the localised groundwater flow direction varies depending on the activity of water abstraction in the southern area. In those cases when the groundwater flows from south to north, pollution which infiltrates from LUs in the northern area may reach the water treatment plant. In other cases, those pollutions may flow with the groundwater towards the southern area instead. These variations (especially in combination with such low measured concentrations of PFAS) make it difficult to determine where the PFAS pollution may come from and where it may migrate.

Additionally, pollution may come from other land uses further away from the study area, which were not included in this analysis. However, if the pollution were to either infiltrate further away or travel with surface water, the measurements made in the southern area should have been higher than the ones made in the immediate study area. This is because both the large-scale groundwater flow in the aquifer (Figure 2) and the surface runoff flow in the watershed for the 100 m buffer (Figure 5) is directed from south to north.

5.2 Method discussion

5.2.1 Watershed Analysis and the D8 Algorithm

The watershed model developed in ArcGIS Pro utilised the D8 (SFD) algorithm, which assigns all flow from a cell to its single steepest downslope neighbour. While the D8 method is a standard, computationally efficient tool for delineating drainage basins, its primary limitation in this study is its tendency to concentrate water into narrow, linear paths (Tarboton, 1997). A study by Behrens (2017) concluded that watersheds delineated with the D8-algorithm often are similar in size to watersheds delineated with the TFM-algorithm (MFD), but that their shape deviates (Behrens, 2017). This suggests that the D8 model may have missed potential overlaps with PFAS-associated LUs that would have been captured by a TFM algorithm, and vice versa. The deviations were, however, found to be minor (Behrens, 2017), supporting the trustworthiness of the calculated watersheds utilising the D8 algorithm in this study.

5.2.2 The Exceedance Duration Tool as a Proxy for Recharge

A study by Akindele et.al (2024) has shown that there is a high likelihood of groundwater recharge in regions which frequently experience flooding. However, it is important to point out that surface water ponding during pluvial floods does not necessarily equal groundwater recharge, it may also heavily dependent on local subsurface conditions and geology. Using PluvioFlow's Exceedance Duration tool (with a 10 cm threshold for 10 minutes) serves as a proxy for identifying depression-focused recharge zones. Depression-focused recharge is not the only form of groundwater recharge, but given the toolsets provided by PluvioFlow and SCALGO, this method was the most robust option available. In addition to missing out on other forms of recharge, this method likely underestimates the recharge occurring on gentle slopes or well-drained soils that do not maintain 10 cm of standing water.

5.2.3 Infiltration Methodology - SCALGO vs. PluvioFlow

The divergence between the SCALGO-based results and the PluvioFlow simulations is fundamentally rooted in how each model handles the relationship between rainfall and soil capacity. While both models aim to quantify the same phenomenon, they operate differently. SCALGO evaluates the ground's instantaneous capacity, whereas PluvioFlow evaluates the accumulated infiltration depth across a dynamic timeline.

The reconstructed SCALGO methodology utilised a static water-balance approach, where the infiltrated depth per pixel is calculated simply as rainfall minus runoff. This simplified water-balance method assumes that all rainfall not being routed away as runoff will infiltrate and does not account for evaporation. As identified in Section 3.5.2.2, this method identifies potential infiltration as an initial loss based on the soil's theoretical storage at a single point in time. It lacks a memory of the rain events' progression. The SCALGO model assumes the rain falls in a single burst, that all infiltration happens instantaneously, and that the soil's capacity to absorb water is a fixed attribute of the landscape. In contrast, the PluvioFlow results are derived from the Accumulated Infiltration Depth recorded over the entire 6-hour simulation (Section 3.5.2.1). This dynamic model tracks the soil's water storage throughout the 3-hour CDS rain event and the subsequent 3-hour period of runoff migration. Crucially, PluvioFlow accounts for saturated soils where once the soil reaches approximately 90 % capacity, the infiltration rate slows to roughly 10 % of its initial rate.

For three out of the six LU Zones (B, C and D), PluvioFlow consistently estimated lower infiltration values compared to SCALGO, while for Zone F, PluvioFlow instead yielded higher infiltration estimations compared to SCALGO. For the two large agricultural fields (Zone A and E), the percent differences switch sign as the rain event intensity increases. (Table 10). PluvioFlow estimates higher infiltration than SCALGO during a 10-year event, only to estimate lower during a 100-year event. An explanation for this may be that, in the 10-year rain event with 32 mm of rain, PluvioFlow's dynamic connectivity allows water to spread across the surface, coming in contact with and infiltrating into a larger area of unsaturated soil over the 6-hour simulation. SCALGO's static approach calculates a single initial loss based on the 32 mm total. This method misses the additional "contact time" provided by the dynamic movement of water across the landscape, potentially leading to the resulting lower estimations of infiltrated volumes. In the 100-year rain event with 54 mm of rain, PluvioFlow's "Saturation Ceiling" may become the dominant factor, since the infiltration rate decays to ~ 10 %, once the soil reaches ~ 90 % capacity. Even though the PluvioFlow calculates infiltration for every pixel, it significantly slows down the intake once the soil is saturated. SCALGO, having no saturation memory, subtracts its full theoretical initial loss from the total 54 mm rainfall, potentially leading to an overestimation of vertical leaching in extreme events. Zone F (cereal industry) remains the exception, with PluvioFlow consistently estimating higher volumes. This suggests that the dynamic routing may be capturing water from surrounding high-elevation ridges and infiltrating it into this industrial zone. SCALGO treats most of the area as an "Artificial" surface due to the Land Cover data being dominated by *Paved Road* and *Buildings* (which has a 100% runoff coefficient), while PluvioFlow on the other hand, still allows for some infiltration in artificial areas that is not buildings (PluvioFlow, 2026a; SCALGO, 2024). The above-discussed saturation approach, which deviates PluvioFlow from SCALGO, may not play as large of a role in Zone F since the total water volume is much smaller, decreasing the risk of saturation. Furthermore, Zone B and D generally exhibit the largest model divergence with percent differences ranging between -44.6 and -58.5. The difference can, in addition to the different methods, mostly be traced back to the differences in the models input layers, land cover and soil type, where the spatial patterns differ quite a bit in there two zones.

Beyond model differences, fundamental limitations in how infiltration translates to actual groundwater recharge must be considered. Firstly, it is important to emphasize that all water calculated as infiltration may not ultimately reach the aquifer as recharge. A portion will inevitably remain retained in the unsaturated vadose zone. Additionally, that the infiltration volumes were calculated across the entirety of each LU zone rather than strictly isolating the identified recharge zones (Figure 6). Consequently, a reservation that the identified zones represent areas of potential surface infiltration rather than verified hydrogeological pathways, needs to be made. Because deep subsurface geological analysis was excluded from the scope of this work, no definitive conclusions can be drawn regarding whether these surface systems are connected to the specific aquifer connected to the MAR basins in the study area. Without empirical geological verification of how the subsurface looks, surface infiltration cannot be assumed to translate directly into aquifer storage. Secondly, human-engineered alterations to the landscape introduce lateral transport pathways not accounted for in the infiltration calculations. The fields (Zone A, C and E) are bordered by a network of drainage ditches (Bermin, 2025), which should be represented by the DEM and therefore accounted for in the calculations, but the depth and location of these can change through time. However, data from municipal records indicates that agricultural field E is equipped with a subsurface tile drainage system, and similar agricultural drainage infrastructure may exist across the other fields. Water is likely to be intercepted and diverted laterally into the ditch network rather than migrating vertically downward toward the groundwater table as assumed in this study. Because these subsurface drainage systems were not integrated into the routing logic of either modelling platform, both models likely underestimate the total volume of water actively routed away from the fields.

5.3 Related Studies

Because this research is structured as a site-specific case study investigating the unique conditions of Gorsingeholm, literature with direct comparability to these exact localised results does not exist. However, the study can be contextualized within a broader academic landscape by drawing parallels to existing research in pluvial flood modelling, localised PFAS source tracking and transport pathways.

5.3.1 Comparison of Hydrological Models

While the specific coupling of PluvioFlow and a re-creation of SCALGO's methodology for source tracking is unique to this study, the broader practice of comparing static and dynamic hydrological models has been established in existing literature (Adhikari, 2020; Andersson, 2021; Barkefors, 2023; Guo et al., 2021; Pihl, 2024). However, these comparative studies evaluate the models through the lens of flood risk analysis, hazard mapping, and municipal infrastructure vulnerability. Instead, this study diverges from standard risk assessment literature by focusing heavily on the underlying infiltration algorithms utilised by the respective model. Rather than merely evaluating surface flooding, this research treats model differences as a tool to explore how instantaneous capacity assumptions versus time-dependent saturation routing impact the identification of potentially polluted groundwater recharge volumes.

5.3.2 Localised PFAS Source Tracking

The pursuit of tracking unknown PFAS contamination to protect municipal drinking water supplies is extensive and explored nationwide. One example is the master thesis of Andersson (2025), also conducted in collaboration with the consulting firm WSP. While sharing the core objective of identifying PFAS contamination migration pathways to safeguard the groundwater, the experimental design differed fundamentally due to the nature of the pollution source. Andersson's study investigated an area with significantly higher baseline concentrations and a known, definitive source, namely a historical firefighting foam (AFFF) training site. Consequently, that research relied on localised spatial source tracking, based on an interpolation of concentration samples, to map out exactly where the pollution had occurred within the facility boundaries, combined with chemical fingerprinting to analyse where specific PFAS compounds were present. In contrast, the Gorsingeholm site presents a much more elusive challenge characterised by low levels, diffuse concentrations without an obvious point source.

5.3.3. PFAS Migration with Surface Runoff and Floodwater

The assumption made in this study, that diffuse PFAS contamination can be rapidly transported by extreme weather events aligns with recent international empirical findings. In surface hydrology, research confirms that the primary mechanism for surface-water PFAS transport is driven by the initial leaching of contaminants from topsoil, followed by lateral transportation via overland flow during intense precipitation events (Borthakur et al., 2021; Dauchy et al., 2019; Richardson et al., 2022). The real-world manifestation of this pathway on a macro-scale was documented during the devastating flash floods in Valencia, Spain in October 2024, where a dramatic post-flood surge of PFAS concentrations was observed in downstream aquatic ecosystems (Rico et al., 2026). This phenomenon occurred partly due to sewerage system failures and partly because extreme pluvial runoff remobilises accumulated, diffuse soil pollutants and rapidly channels them into drainage networks and surface water bodies, where the contaminants settle and accumulate. Rico et al's study supported the decision in this study to stress-test the Gorsingeholm landscape using 10-year and 100-year return periods.

5.4 Future Studies and Improvements

While this study provides a foundational spatial risk assessment for PFAS pathways at Gorsingeholm, several methodological boundaries and limitations highlight critical avenues for future research. To refine the predictive accuracy of location contaminant transport modelling, future spatial analyses should prioritise calculating the percentage of groundwater recharge zones intersecting each land use relative to specific zone's total area. Normalising these areas as a proportion of total land use will allow for an unbiased, and direct comparison of recharge potential across highly contrasting land-use archetypes, regardless of their total spatial extent. Furthermore, due to constraints in model harmonisation, infiltration volumes in this study were aggregated across entire land use areas. Future work should isolate and calculate infiltration volumes strictly within the boundaries of the identified depression-focused recharge zones to eliminate surrounding unflooded pixels from the volumetric sum, yielding a more precise quantification of localised leaching potential. Detailed analysis of groundwater dynamics and flow, e.g. groundwater modelling, to improve understanding of where infiltrated pollution may migrate, would also be of interest in future studies

To further understand the physical drivers of these systems, a statistical correlation analysis could be executed to link modelled infiltration depths directly to underlying soil types and land cover data. Investigating whether these correlations remain consistent or diverge between SCALGO and PluvioFlow can help determine which landscape parameters intro the greatest variance between the models. Additionally, because this research quantified volumes exclusively for subsurface infiltration, future modelling should also quantify total lateral surface runoff volumes to fully map the potential transport of PFAS. Comparing volumetric runoff against infiltrated water is essential to determine whether the primary pathway for contaminants migration during extreme rain and pluvial flooding events is driven by lateral surface routing or vertical groundwater recharge.

To fully exploit the hydrodynamic capabilities of PluvioFlow, future studies should move beyond the final simulation timestep analysed in this report and evaluate the complete temporal progression and surface water velocity throughout the entire simulation window. This temporal analysis would clarify exactly when and how fast contaminant pathways are activated during a storm event. Beyond summer rainfall scenarios, future research should also incorporate seasonal snowmelt dynamics by analysing winter accumulation and spring thaw scenarios. Investigate if there is snow deposit sites in the study areas, since this could capture the potential release of concentrated, short-term PFAS pulses accumulated in ploughed snow piles in built-up zones, which traditional rainfall models inherently omit. Finally, these theoretical risk profiles must be validated through targeted empirical sampling, which should involve collecting soil cores, surface- and groundwater samples specifically within the neighbouring land uses and activities.

6 Conclusion

By working to improve the understanding of surface water flow patterns and groundwater recharge zones in Gorsingeholm and connecting these findings with potential PFAS-associated land uses, this study provides valuable insight into contaminant pathways and sources.

This study demonstrates that surface runoff into the water treatment plant originate from the southeastern proximity for the immediate study area, 10 m and 50 m buffer zones, while it may originate from approximately 8 km southwest in a “worst-case” precautionary scenario when a 100 m buffer was analysed. The specific land uses located within these runoff paths are the cereal industry (F), the farmstead/SME (D), and the southwestern field (E), while the other nearby land uses fields (A and C) and households (B) remained hydrologically disconnected.

Additionally, the spatial distribution of groundwater recharge zones during rainfall events with medium to long return periods is heavily concentrated within the flat topography of the agricultural fields and localized built-up depressions. Looking at the areal extent of these zones within neighbouring land uses, the potential groundwater recharge areas are largest in the massive agricultural fields of Zones A and E. However, when evaluating their relative footprints, Zone C (agricultural field) and Zone D (farmstead/SME) also exhibit large recharge zones in proportion to their smaller total land use areas. All areas were continuously larger for the 100-year rain event compared to the 10-year rain event.

Furthermore, the volumetric contributions of infiltrated water from each land use vary largely based on spatial scale and soil characteristics. The two large agricultural fields (A and E) act as the dominant contributors to the total volume of potentially infiltrated water to the groundwater, which is mostly a function of their massive size. Conversely, Zone F (cereal industry) demonstrates the lowest infiltration intensity, suggesting this area is dominated by surface runoff rather than infiltration.

Finally, a synthesis of literature links these contributing pathways to historical and active PFAS usage signatures. The cereal industry (F) is officially categorised as an industry associated with potential ground pollution and pesticide applications. The farmstead/SME accommodates a business for recreational boat and car storage, which is classified as a potential PFAS industry associated with PFAS contamination in both ground and sediment. Furthermore, the agricultural fields (A, C, and E) are commonly associated with diffuse PFAS accumulation through the application of sewage sludge as fertilizer and the use of specific pesticide compounds. households (B) are not associated with significant PFAS-usage known to affect nearby outdoor environments.

Despite these potential associations, a definite origin for the elevated PFAS levels could not be definitively identified within this study. This research underscores the necessity of considering pluvial flooding as a transport mechanism, as extreme weather events are capable of mobilising and concentrating these otherwise diffuse pollutants through rapid hydrological activation. Given these dynamics, future efforts should prioritise targeted investigation and sampling in the cereal industry (F) primarily via surface runoff pathways, and the farmstead/SME (D) regarding both surface runoff and groundwater recharge. Ultimately, while this study does not confirm a specific source, it provides a diagnostic framework and identifies high-priority areas that should be the focus of future investigative monitoring.

Footnotes

[1] Basemap created by Esri, using World Imagery [Basemap], 2026. Sources: Esri, DigitalGlobe, GeoEye, i-cubed, USDA FSA, USGS, AEX, Getmapping, Aerogrid, IGN, IGP, swisstopo, and the GIS User Community

References

Ackerman Grunfeld, D., Gilbert, D., Hou, J., Jones, A. M., Lee, M. J., Kibbey, T. C. G., & O'Carroll, D. M. (2024). Underestimated burden of per- and polyfluoroalkyl substances in global surface waters and groundwaters. *Nature Geoscience*, *17*(4), 340–346. https://doi.org/10.1038/s41561-024-01402-8

Adhikari, U. (2020). *Master's thesis in Infrastructure and Environmental Engineering* [Master degree thesis]. Chalmers University of Technology.

Ahmed, M. B., Johir, M. A. H., McLaughlan, R., Nguyen, L. N., Xu, B., & Nghiem, L. D. (2020). Per- and polyfluoroalkyl substances in soil and sediments: Occurrence, fate, remediation and future outlook. *Science of The Total Environment*, *748*, 141251. https://doi.org/10.1016/j.scitotenv.2020.141251

Ahrens, L., Hedlund, J., Dürig, W., & Trö, R. (2016). *Screening of PFASs in groundwater and surface water* (2026:2). Sveriges lantbruksuniversitet, Institutionen för vatten och miljö.

Akindele, A., Akinyele, I., Akande, A., Jolaosho, A., Olusami, J., Familusi, A., Olatunji, A., & Ogundare, D. (2024). *Effect of Flooding on Groundwater Recharge Potential Using GIS Techniques*. *7*, 3048–5215. https://doi.org/10.5281/zenodo.13859313

AMS. (n.d.). *Return period*. American Meteorological Society [AMS]. Glossary of Meteorology. Retrieved 16 May 2026, from https://glossary.ametsoc.org/wiki/return-period/

Andersson, A., Andersson, B., Gerdtsson, A., Malm, G., & Wiik, L. (n.d.). *Konsekvensutredning avseende utfasning av växtskyddsmedel med verksamma ämnen som kan bilda trifluorättiksyra (TFA): Potatisodling i Sverige*. Jordbruksverket. Retrieved 16 May 2026, from https://jordbruksverket.se/download/18.603f70b719cd5b3b941171f/1773241139914/Konsekvensutredning-pfas-potatis-tga.pdf

Andersson, E. (2021). *Flood modelling in urban areas: A comparative study of MIKE 21 and SCALGO Live* [KTH Royal Institute of Technology]. https://www.diva-portal.org/smash/get/diva2:1589915/FULLTEXT01.pdf

Andersson, J. (2025). *Kartläggning av spridningsmönstret för PFAS11 kring en brandövningsplats*. Lund University.

Barkefors, D. (2023). *The influence of infiltration capacity and antecedent soil moisture conditions on urban pluvial flooding*. Uppsala University.

Behrens, I. (2017). *Watershed delineation for runoff estimations to culverts in the Swedish road network—A comparison between two GIS based hydrological modelling methods and a manually delineated watershed* [Master degree thesis, Lund University]. https://lup.lub.lu.se/luur/download?func=downloadFile&recordOId=8918382&fileOId=8918388

Bermin, J. (2025). *Bedömning av möjliga PFAS källor: Vattenskyddsområde Gorsingeholm* (No. 10356184). WSP Sverige AB.

Biswas, B., Joseph, A., Parveen, N., Ranjan, V. P., Goel, S., Mandal, J., & Srivastava, P. (2025). Contamination of per- and poly-fluoroalkyl substances in agricultural soils: A review. *Journal of Environmental Management*, *380*, 124993. https://doi.org/10.1016/j.jenvman.2025.124993

Bolagsverket. (n.d.). *Sök företag – Sök företagsinformation*. Bolagsverket. Företagsinfo. Retrieved 6 May 2026, from https://foretagsinfo.bolagsverket.se/sok-foretagsinformation-web/foretag

Borthakur, A., Wang, M., He, M., Ascencio, K., Blotevogel, J., Adamson, D. T., Mahendra, S., & Mohanty, S. K. (2021). Perfluoroalkyl acids on suspended particles: Significant transport pathways in surface runoff, surface waters, and subsurface soils. *Journal of Hazardous Materials*, *417*, 126159. https://doi.org/10.1016/j.jhazmat.2021.126159

Boström, G., Tröger, R., Jonsson, O., & Gönczi, M. (2024). *Identifiering av metaboliter från växtskyddsmedel relevanta att analysera i svenska yt- och grundvatten* (2024:1). SLU Centre for Pesticides in the Environment, Swedish University of Agricultural Sciences. https://doi.org/10.54612/a.642p6k0i4n

Brusseau, M. L., Anderson, R. H., & Guo, B. (2020). PFAS concentrations in soils: Background levels versus contaminated sites. *Science of The Total Environment*, *740*, 140017. https://doi.org/10.1016/j.scitotenv.2020.140017

Buck, R. C., Franklin, J., Berger, U., Conder, J. M., Cousins, I. T., de Voogt, P., Jensen, A. A., Kannan, K., Mabury, S. A., & van Leeuwen, S. P. (2011). Perfluoroalkyl and polyfluoroalkyl substances in the environment: Terminology, classification, and origins. *Integrated Environmental Assessment and Management*, *7*(4), 513–541. https://doi.org/10.1002/ieam.258

Commission Recommendation of 6 May 2003 Concerning the Definition of Micro, Small and Medium-Sized Enterprises, 2003/361/EC (2003). https://eur-lex.europa.eu/legal-content/EN/TXT/PDF/?uri=CELEX:32003H0361

Cousins, I. T., Johansson, J. H., Salter, M. E., Sha, B., & Scheringer, M. (2022). Outside the Safe Operating Space of a New Planetary Boundary for Per- and Polyfluoroalkyl Substances (PFAS). *Environmental Science & Technology*, *56*(16), 11172–11179. https://doi.org/10.1021/acs.est.2c02765

Dahlström, B. (2010). *Regnintensitet – en molnfysikalisk betraktelse* (No. 2010-05). Svenskt Vatten Utveckling.

Dalahmeh, S., Tirgani, S., Komakech, A. J., Niwagaba, C. B., & Ahrens, L. (2018). Per- and polyfluoroalkyl substances (PFASs) in water, soil and plants in wetlands and agricultural areas in Kampala, Uganda. *Science of The Total Environment*, *631–632*, 660–667. https://doi.org/10.1016/j.scitotenv.2018.03.024

Dauchy, X., Boiteux, V., Colin, A., Bach, C., Rosin, C., & Munoz, J.-F. (2019). Poly- and Perfluoroalkyl Substances in Runoff Water and Wastewater Sampled at a Firefighter Training Area. *Archives of Environmental Contamination and Toxicology*, *76*(2), 206–215. https://doi.org/10.1007/s00244-018-0585-z

Directive (EU) 2020/2184 of the European Parlament and of the Council of 16 December 2020 on the Quality of Water Intended for Human Consumption, 2020/2184 (2020). https://eur-lex.europa.eu/legal-content/EN/TXT/PDF/?uri=CELEX:32020L2184

Earon, R. (2025). *Spridning av PFAS i grundvatten: Simulerade halter över tid i en teoretisk grundvattentäkt* (Diarienr: 3.1.2-2401-0173; p. 35). Statens geotekniska institut [SGI].

EFSA CONTAM Panel (EFSA Panel on Contaminants in the Food Chain), Schrenk, D., Bignami, M., Bodin, L., Chipman, J. K., del Mazo, J., Grasl-Kraupp, B., Hogstrand, C., Hoogenboom, L. (Ron), Leblanc, J., Nebbia, C. S., Nielsen, E., Ntzani, E., Petersen, A., Sand, S., Vleminckx, C., Wallace, H., Barregård, L., Ceccatelli, S., … Schwerdtle, T. (2020). Risk to human health related to the presence of perfluoroalkyl substances in food. *EFSA Journal*, *18*(9). https://doi.org/10.2903/j.efsa.2020.6223

Esri. (2023a). *ArcGIS Pro* (Version 3.2.0) [Computer software]. Environmental Systems Research Institute [Esri].

Esri. (2023b, July 27). *How To: Create a Watershed Model Using Hydrology in ArcGIS Pro*. Environmental Systems Research Institute [Esri]. https://support.esri.com/en-us/knowledge-base/how-to-create-a-watershed-model-using-hydrology-in-arcg-000023169

European Chemical Agency. (n.d.). *Per- and polyfluoroalkyl substances (PFAS)*. European chemical agency [ECHA]. Retrieved 2 February 2026, from https://echa.europa.eu/hot-topics/perfluoroalkyl-chemicals-pfas

Fredriksson, F., Eriksson, U., Kärrman, A., & Yeung, L. W. Y. (2022). Per- and polyfluoroalkyl substances (PFAS) in sludge from wastewater treatment plants in Sweden—First findings of novel fluorinated copolymers in Europe including temporal analysis. *Science of The Total Environment*, *846*, 157406. https://doi.org/10.1016/j.scitotenv.2022.157406

Ghisi, R., Vamerali, T., & Manzetti, S. (2019). Accumulation of perfluorinated alkyl substances (PFAS) in agricultural plants: A review. *Environmental Research*, *169*, 326–341. https://doi.org/10.1016/j.envres.2018.10.023

Glüge, J., Scheringer, M., Cousins, I. T., DeWitt, J. C., Goldenman, G., Herzke, D., Lohmann, R., Ng, C. A., Trier, X., & Wang, Z. (2020). An overview of the uses of per- and polyfluoroalkyl substances (PFAS). *Environmental Science: Processes & Impacts*, *22*(12), 2345–2373. https://doi.org/10.1039/D0EM00291G

Google. (n.d.-a). *Map view over Gorsingeholm* [Google Maps]. Retrieved 18 May 2026, from https://www.google.com/maps/search/gorsingeholm

Google. (n.d.-b). *Strängnäs Båt & Bilförvaring* [Google Maps]. Retrieved 18 May 2026, from https://www.google.com/maps/place/Str%C3%A4ngn%C3%A4s+B%C3%A5t+%26+Bilf%C3%B6rvaring/@59.3567232,16.9423417,11383m/data=!3m1!1e3!4m6!3m5!1s0x465efdffcc309789:0xb696f3229609088f!8m2!3d59.3518928!4d17.0526736!16s%2Fg%2F11w39v075r?entry=ttu&g_ep=EgoyMDI2MDUxMy4wIKXMDSoASAFQAw%3D%3D

Guo, K., Guan, M., & Yu, D. (2021). Urban surface water flood modelling – a comprehensive review of current models and future challenges. *Hydrology and Earth System Sciences*, *25*(5), 2843–2860. https://doi.org/10.5194/hess-25-2843-2021

ITRC. (2023). *Fate and Transport of Per- and Polyfluoroalkyl Substances (PFAS)*. Interstate Technology & Regulatory Council [ITRC]. https://pfas-1.itrcweb.org/wp-content/uploads/2023/10/FT_PFAS_FactSheet_Sept2023_final.pdf

ITRC. (2026). *PFAS Technical and Regulatory Guidance Document and Fact Sheets* (PFAS-1). Interstate Technology & Regulatory Council, PFAS Team [ITRC]. https://pfas-1.itrcweb.org/

Kannan, U., Ravichandran, M. K., Monisha, M., Krishnasamy, S., Valliammai, Prabakar, P., Darshini, D., & Sunantha, G. (2026). Short-chain PFAS: A global challenge - Environmental fate, health risks, and promising removal technologies. *Results in Chemistry*, *20*, 103000. https://doi.org/10.1016/j.rechem.2025.103000

Kärrman, A., Fredriksson, F., & Särnholm, E. (2024). *Slamspridning på åkermark – PFAS i slam, jord, gröda och mask* (Nos 2024–5; p. 41). Svenskt Vatten AB.

Keifer, C. J., & Chu, H. H. (1957). Synthetic Storm Pattern for Drainage Design. *Journal of the Hydraulics Division*, *83*(4), 1332–25. https://doi.org/10.1061/JYCEAJ.0000104

KEMI. (2024a). *Gränsvärden och riktvärden för PFAS*. Kemikalieinspektionen [KEMI]. https://www.kemi.se/download/18.db1a89d18b37a78175b303/1707489966084/Gransvarden-och-riktvarden-for-PFAS.pdf

KEMI. (2024b, November 3). *PFAS i vardagsvaror – råd till privatpersoner*. Kemikalieinspektionen [KEMI]. https://www.kemi.se/rad-till-privatpersoner/kemikalier-i-material/pfas-i-vardagsvaror---rad-till-privatpersoner

KEMI. (2025). *Verksamma ämnen i biocidprodukter som är PFAS*. Kemikalieinspektionen [KEMI]. https://www.kemi.se/lagar-och-regler/lagstiftningar-inom-kemikalieomradet/bekampningsmedel/biocider/verksamma-amnen/verksamma-amnen-i-biocidprodukter-som-ar-pfas

KEMI. (2026a). *Verksamma ämnen i växtskyddsmedel som är PFAS*. Kemikalieinspektionen [KEMI]. https://www.kemi.se/lagar-och-regler/lagstiftningar-inom-kemikalieomradet/bekampningsmedel/vaxtskyddsmedel/aktuellt-om-vaxtskyddsmedel/verksamma-amnen-i-fokus/verksamma-amnen-i-vaxtskyddsmedel-som-ar-pfas

KEMI. (2026b, February 19). *PFAS*. Kemikalieinspektionen [KEMI]. https://www.kemi.se/hallbarhet/amnen-och-material/pfas

Koliokosta, E. (2023). Return Periods in Assessing Climate Change Risks: Uses and Misuses. *Environmental Sciences Proceedings*, *26*(1), 75. https://doi.org/10.3390/environsciproc2023026075

Länsstyrelsen Södermanlands län. (n.d.). *Kartor över miljöfarlig verksamhet*. Länsstyrelsen Södermanlands län. Retrieved 16 May 2026, from https://www.lansstyrelsen.se/sodermanland/miljo-och-vatten/miljofarlig-verksamhet/kartor-over-miljofarlig-verksamhet.html

Länsstyrelserna. (2020). *LST NikITa Tillståndspliktiga miljöfarliga verksamheter – punkter* [Webb GIS]. https://ext-geoportal.lansstyrelsen.se/arcgis/apps/experiencebuilder/experience/?draft=true&id=bab2e5bb59bc404cb54328625920aa5f

Länsstyrelserna. (2025). *LST Potentiellt förorenade områden EBH - karttjänst* [Webb GIS]. https://ext-webbgis.lansstyrelsen.se/lst_ebh_karta/

Lantmäteriet. (2025). *Nationell dataproduktspecifikation Grid* (Version informationsspecifikation-Grid-1-0-Test-1-3). Lantmäteriet.

Lea, N. J. (1992). An Aspect-Driven Kinematic Routing Algorithm. In *Overland Flow*. CRC Press.

Li, H., Dong, Q., Zhang, M., Gong, T., Zan, R., & Wang, W. (2023). Transport behavior difference and transport model of long- and short-chain per- and polyfluoroalkyl substances in underground environmental media: A review. *Environmental Pollution*, *327*, 121579. https://doi.org/10.1016/j.envpol.2023.121579

Lindstrom, A. B., Strynar, M. J., Delinsky, A. D., Nakayama, S. F., McMillan, L., Libelo, E. L., Neill, M., & Thomas, L. (2011). Application of WWTP Biosolids and Resulting Perfluorinated Compound Contamination of Surface and Well Water in Decatur, Alabama, USA. *Environmental Science & Technology*, *45*(19), 8015–8021. https://doi.org/10.1021/es1039425

Livsmedelsverket. (2026, January 27). *PFAS - Per- och polyfluorerade alkylsubstanser*. Livsmedelsverket. https://www.livsmedelsverket.se/livsmedel-och-innehall/oonskade-amnen/miljogifter/pfas-poly-och-perfluorerade-alkylsubstanser

Livsmedelsverkets föreskrifter om dricksvatten, LIVSFS 2022:12 (2023). https://www.livsmedelsverket.se/4af3b1/globalassets/om-oss/lagstiftning/dricksvatten---naturl-mineralv---kallv/livsfs-2022-12_web_t.pdf

Lopes da Silveira, A. L. (2016). Cumulative equations for continuous time Chicago hyetograph method. *RBRH*, *21*, 646–651. https://doi.org/10.1590/2318-0331.011615094

Lundkvist, A., Gilbertsson, M., Pedersen, M., & Andersson, R. (n.d.). *Konsekvensutredning avseende utfasning av växtskyddsmedel med verksamma ämnen som kan bilda trifluorättiksyra (TFA): Herbicider i svensk jordbruks- och trädgårdsproduktion*. Retrieved 17 May 2026, from https://jordbruksverket.se/download/18.603f70b719cd5b3b941171d/1773241139807/Konsekvensutredning-pfas-herbicider-tga.pdf

Maldonado, L. (2021). *Gorsingeholms grundvattenskyddsområde: Utredning inducerad infiltration* (No. 10249015). WSP Environmental Sverige.

Maldonado, L., & Tagesson, E. (2025). *Vattenskyddsområde Gorsingeholm: Tekniskt undelag—Beslutsunderlag* (No. 10249015). WSP Sverige AB.

MSB. (2023). *Metod för skyfallskartering av tätorter* ([Guidance] No. MSB2260). Myndigheten för samhällsskydd och beredskap [MSB].

Naturskyddsföreningen. (2024, November 7). *PFAS i bekämpningsmedel*. Naturskyddsföreningen. https://www.naturskyddsforeningen.se/artiklar/pfas-i-bekampningsmedel/

NVV. (2025a). *Branschlistan förorenade områden*. Naturvårdsverket [NVV]. https://www.naturvardsverket.se/490731/globalassets/vagledning/fororenade-omraden/inventering/branschlistan-fororenade-omraden-ar-2025.pdf

NVV. (2025b). *Kunskap om PFAS i livsmedel och miljö* (NV-09898-21). Naturvårdsverket [NVV].

Olsson, J., Berg, P., Eronn, A., Simonsson, L., Södling, J., Wern, L., & Yang, W. (2017). *Extremregn i nuvarande och framtida klimat* (No. 47; Klimatologirapport). SMHI.

Persson, A., Pilesjö, P., & Hasan, A. (2024). Dynamic modeling of urban hydrology in a geographic information system-setting with TFM-DYN. In *Geographical Information Science* (pp. 315–336). Elsevier. https://doi.org/10.1016/B978-0-443-13605-4.00004-7

Pihl, V. (2024). *Resurseffektivare användning av dagvattenmodeller*. Lund University.

Pilesjö, P., & Hasan, A. (2014). A Triangular Form-based Multiple Flow Algorithm to Estimate Overland Flow Distribution and Accumulation on a Digital Elevation Model. *Transactions in GIS*, *18*(1), 108–124. https://doi.org/10.1111/tgis.12015

PluvioFlow. (2026a). *PluvioFlow* (Version 2026.03.19) [Computer software]. PluvioFlow. https://pluvioflow.com/

PluvioFlow. (2026b). *Skyfallskartering: Metodrapport* (Version 2026.02.11).

Rakhecha, P., & Singh, V. P. (2010). Statistical Analysis of Precipitation. In *Applied Hydrometeorology* (pp. 244–277). Springer Science & Business Media.

Richardson, M. J., Kabiri, S., Grimison, C., Bowles, K., Corish, S., Chapman, M., & McLaughlin, M. J. (2022). Per- and Poly-Fluoroalkyl Substances in Runoff and Leaching from AFFF-Contaminated Soils: A Rainfall Simulation Study. *Environmental Science & Technology*, *56*(23), 16857–16865. https://doi.org/10.1021/acs.est.2c05377

Rico, A., Picazo, A., Chavez, J., Campo, J., Colomer-Vidal, P., Muñoz-Arnanz, J., Jiménez, B., Rizzi, C., Federico, L., Villa, S., Palacios, J. F., Rochera, C., Amador, P., & Camacho, A. (2026). Impacts of the 2024 flash flood on water quality, pathogenic bacteria and organic contaminant risks in the Albufera Natural Park (Valencia, Spain). *Environmental Research*, *290*, 123515. https://doi.org/10.1016/j.envres.2025.123515

SCALGO. (n.d.-a). *Chicago Design Storm*. SCALGO. SCALGO Live Documentation. Retrieved 16 May 2026, from https://scalgo.com/en-US/scalgo-live-documentation/soil-vegetation-atmosphere-properties/rain-events/chicago-design-storm

SCALGO. (n.d.-b). *Country Specific—Sweden*. SCALGO. SCALGO Live Documentation. Retrieved 16 May 2026, from https://scalgo.com/en-US/scalgo-live-documentation/country-specific/sweden

SCALGO. (n.d.-c). *Flash Flood Map*. SCALGO. SCALGO Live Documentation. Retrieved 16 May 2026, from https://scalgo.com/en-US/scalgo-live-documentation/analysis/flash-flood-map

SCALGO. (n.d.-d). *Physical Properties—Land Cover*. SCALGO. SCALGO Live Documentation. Retrieved 16 May 2026, from https://scalgo.com/en-US/scalgo-live-documentation/soil-vegetation-atmosphere-properties/land-cover

SCALGO. (n.d.-e). *Physical Properties—Soil Types*. SCALGO. SCALGO Live Documentation. Retrieved 16 May 2026, from https://scalgo.com/en-US/scalgo-live-documentation/soil-vegetation-atmosphere-properties/soil

SCALGO. (2024). *Whitepaper: The Rainfall-Runoff Model in the Flash Flood Map in SCALGO Live Sweden* (Version 1.2). SCALGO. https://scalgo.com/uploads/documentation/Whitepaper-RRM-SE.pdf

Shah, S. M. H., Al-Qadami, E., Abdulazeez, I., Yassin, M. A., Abba, S. I., Lawal, D. U., & Aljundi, I. H. (2025). Per- and polyfluoroalkyl substances (PFASs) in water-based environments: A systematic review of treatment technologies and research trends

(2017–2024). *Journal of Fluorine Chemistry*, *283–284*, 110435. https://doi.org/10.1016/j.jfluchem.2025.110435

SMHI. (n.d.-a). *Skyfall och rotblöta*. Sveriges meteorologiska och hydrologiska institut [SMHI]. SMHIs Kunskapsbank. Retrieved 16 May 2026, from https://www.smhi.se/kunskapsbanken/meteorologi/skyfall-och-hagel/skyfall-och-rotblota

SMHI. (n.d.-b). *Statistik för extrema korttidsregn – skyfall*. Sveriges meteorologiska och hydrologiska institut [SMHI]. SMHIs Kunskapsbank. Retrieved 27 February 2026, from https://www.smhi.se/kunskapsbanken/meteorologi/skyfall-och-hagel/statistik-for-extrema-korttidsregn---skyfall

SMHI. (2017). *Sammanfattning till extremregn i nuvarande och framtida klimat* (No. 47; Klimatologirapport). Sveriges meteorologisa och hydrologiska institut [SMHI].

SMHI. (2025, September 24). *Skyfallsstatistik: Regional statistik för extrema korttidsregn*. https://www.smhi.se/klimat/framtidens-klimat/skyfallsstatistik-regional-statistik-for-extrema-korttidsregn

Sparrenbom, C., & Jeppsson, H. (Eds). (2022). *Grundvattenboken* (1st edn). Studentlitteratur.

Strängnäs Båt & Bilförvaring. (n.d.). *Fordonsförvaring—Vinteruppställning i kallhall och varmhall i Strängnäs*. Vinteruppställning. Retrieved 18 May 2026, from https://vinteruppstallning.se/

Svenskt Vatten. (2016). *Avledning av dag- drän- och spillvatten: Funktionskrav, hydraulisk dimensionering och utformning av allmänna avloppssystem* (No. P110-Del 1). Svenskt Vatten AB. https://vav.griffel.net/filer/p110_del1_jan2016.pdf

Tarboton, D. G. (1997). A new method for the determination of flow directions and upslope areas in grid digital elevation models. *Water Resources Research*, *33*(2), 309–319. https://doi.org/10.1029/96WR03137

Appendix

Below is a list of abbreviations for all PFAS compounds mentioned in this study:

PFAS	Per- and polyfluoroalkyl substances
PFAA	Perfluoroalkyl acids
PFSA	Perfluoroalkane sulfonic acids
PFBS	Perfluorobutanesulfonic acid
PFPS	Perfluoropentanesulfonic acid
PFHxS	Perfluorohexanesulfonic acid
PFHpS	Perfluoroheptanesulfonic acid
PFOS	Perfluorooctanesulfonic acid
PFNS	Perfluorononanesulfonic acid
PFDS	Perfluorodecanesulfonic acid
PFUnDS	Perfluoroundecanesulfonic acid
PFDoDS	Perfluorododecanesulfonic acid
PFTrDS	Perfluorotridecanesulfonic acid
PFCA	Perfluoralkyl carboxylic acids
PFBA	Perfluorobutanoic acid
PFPA	Perfluoropentanoic acid
PFHxA	Perfluorohexanoic acid
PFHpA	Perfluoroheptanoic acid
PFOA	Perfluorooctanoic acid
PFNA	Perfluorononanoic acid
PFDA	Perfluorodecanoic acid
PFUnDA	Perfluoroundecanoic acid
PFDoDA	Perfluorododecanoic acid
PFTrDA	Perfluorotridecanoic acid
TFA	Trifluoroacetic acid
Telomers	
6:2 FTS	6:2 Fluorotelomersulfonic acid